TopBP1 utilises a bipartite GINS binding mode to support genome replication

Matthew Day[*,1,2,+], Bilal Tetik[*,3], Milena Parlak[*,3], Yasser Almeida-Hernández[4,5], Markus Räschle[6], Farnusch Kaschani[7,8], Heike Siegert[3], Anika Marko[3], Elsa Sanchez-Garcia[4,5], Markus Kaiser[7,8], Isabel A. Barker[2], Laurence H. Pearl[2,9,+], Antony W. Oliver[2,+], Dominik Boos[3,+]

[1], School of Biological and Behavioural Sciences, Blizard Institute, Queen Mary University of London, London, E1 2AT, UK

[2], Cancer Research UK DNA Repair Enzymes Group, Genome Damage and Stability Centre, School of Life Sciences, University of Sussex, Falmer, Brighton BN1 9RQ, UK

[3], Molecular Genetics II, Center of Medical Biotechnology, University of Duisburg-Essen, Universitätsstraße 2-5, 45141 Essen, Germany

[4], Computational Bioengineering, Fakultät Bio- und Chemieingenieurwesen, Technical University Dortmund, Emil-Figge Str. 66, 44227 Dortmund, Germany

[5], Computational Biochemistry, Center of Medical Biotechnology, University of Duisburg-Essen, Universitätsstraße 2-5, 45141 Essen, Germany

[6], Molecular Genetics, Technical University Kaiserslautern, Paul-Ehrlich Straße 24, 67663 Kaiserslautern, Germany

[7], Analytics Core Facility Essen, Center of Medical Biotechnology, University of Duisburg-Essen, Universitätsstraße 2-5, 45141 Essen, Germany

[8], Chemical Biology, Center of Medical Biotechnology, University Duisburg-Essen, Fakultät Biologie, Essen, Germany

[9], Division of Structural Biology, Institute of Cancer Research, Chester Beatty Laboratories, 237 Fulham Road, London SW1E 6BT, UK

[*] equal contribution
[+] corresponding authors:
Mathew Day: matthew.day@qmul.ac.uk
Laurence H. Pearl: Laurence.Pearl@sussex.ac.uk
Antony W. Oliver: Antony.Oliver@sussex.ac.uk
Dominik Boos: dominik.boos@uni-due.de

Abstract

Activation of the replicative Mcm2-7 helicase by loading GINS and Cdc45 is crucial for replication origin firing, and as such for faithful genetic inheritance. Our biochemical and structural studies demonstrate that the helicase activator GINS interacts with TopBP1 through two separate binding surfaces, the first involving a stretch of highly conserved amino acids in the TopBP1-GINI region, the second a surface on TopBP1-BRCT4. The two surfaces bind to opposite ends of the A domain of the GINS subunit Psf1. Mutation analysis reveals that either surface is individually able to support TopBP1-GINS interaction, albeit with reduced affinity. Consistently, either surface is sufficient for replication origin firing in *Xenopus* egg extracts and becomes essential in the absence of the other. The TopBP1-GINS interaction appears sterically incompatible with simultaneous binding of DNA polymerase epsilon (Polε) to GINS when bound to Mcm2-7-Cdc45, although TopBP1-BRCT4 and the Polε subunit PolE2 show only partial competitivity in binding to Psf1. Our TopBP1-GINS model improves the understanding of the recently characterised metazoan pre-loading complex. It further predicts the coordination of three molecular origin firing processes, DNA polymerase epsilon arrival, TopBP1 ejection and GINS integration into Mcm2-7-Cdc45.

Introduction

Duplicating the genome accurately and exactly once each cell cycle lies at the heart of faithful genetic inheritance. The effective execution and regulation of DNA replication origin firing is pivotal to accurate genome duplication. Our understanding of how origin firing in eukaryotes generates replisomes from their inactive precursors, pre-replicative complexes that comprise double hexamers of the Mcm2-7 helicase (MCM-DH), has increased. However, how the two helicase activators GINS and Cdc45 are loaded onto MCM-DHs remains less well understood.

MCM-DHs form during origin licensing in the G1 phase of the cell cycle when the activity level of cyclin-dependent kinases (CDKs) are low [1]. A set of essential licensing factors sequentially loads two Mcm2-7 helicase hexamers onto origin DNA. Double-stranded DNA passes through the central channels of these helicase-inactive MCM-DHs [2, 3, 4]. In the following S phase, high CDK activity induces origin firing, converting each MCM-DH into two replisomes travelling in opposite directions. During this process, the MCM-DH separates, helicase activity is switched on, the dsDNA running inside the hexamers is unwound, and what will become the single lagging strand DNA template is excluded from each hexamer (Supplementary Fig. 1). The two active helicases pass each other, engaging with the DNA fork with their respective N-terminal faces first [5, 6].

Mcm2-7 helicase activation involves the loading of Cdc45 and GINS onto MCM-DHs to form the CMG (Cdc45-Mcm2-7-GINS) helicase [7, 8, 9, 10]. CMG assembly occurs tightly coupled with partial Mcm2-7 double hexamer splitting and limited untwisting of the dsDNA inside the central CMG channels [6, 11, 12]. The subsequent assembly of mature replisomes involves several steps and many additional replisome components [6, 10].

In budding yeast, Cdc45 and GINS integration requires Dbf4-dependent kinase (DDK), S-CDK, the Sld3-Sld7 protein complex (Treslin-MTBP in higher eukaryotes), Dpb11 (TopBP1), Sld2 (potential human equivalents RecQL4 and DONSON) and DNA polymerase epsilon (DNA Polε) [10, 13, 14]. DDK binds MCM-DHs and phosphorylates the Mcm2-7 helicase, allowing Sld3-Sld7$^{\text{Treslin-MTBP}}$ association [15, 16, 17]. MCM-DH-bound Sld3-Sld7$^{\text{Treslin-MTBP}}$ recruits Cdc45 involving a direct Sld3^{Treslin}-Cdc45 interaction [14, 18, 19]. Sld3-Sld7$^{\text{Treslin-MTBP}}$ is also involved in recruiting Dpb11$^{\text{TopBP1}}$. For this, S-CDK phosphorylates Sld3^{Treslin} on conserved CDK consensus sites, which can then bind to the N-terminal BRCT (breast cancer type 1 susceptibility) domains of Dpb11$^{\text{TopBP1}}$ [20, 21, 22] (Fig. 1a(i)). The interaction between Sld3^{Treslin} and Dpb11$^{\text{TopBP1}}$ serves to recruit the pre-loading complex (pre-LC) to MCM-DHs, comprising Dpb11$^{\text{TopBP1}}$, GINS, Sld2$^{\text{RecQL4/DONSON}}$ and DNA Polε [23]. Pre-LC integrity requires a CDK phosphorylation-mediated interaction between phosphorylated Sld2$^{\text{RecQL4/DONSON}}$ and the C-terminal BRCT-pair of Dpb11$^{\text{TopBP1}}$ (Fig. 1a(i)). Sld2$^{\text{RecQL4/DONSON}}$, Dpb11$^{\text{TopBP1}}$ and Sld3-Sld7$^{\text{Treslin-MTBP}}$ then detach from the origin-bound Mcm2-7 [13, 24], leaving GINS and Cdc45 behind to form the CMG helicase. DNA Polε associates with CMG in a dynamic fashion to form the CMGE complex (CMG-DNA Polε) [25]. The N-terminus of the Dpb2 subunit of DNA Polε and its vertebrate equivalent PolE2 bind to the Psf1 subunit of GINS [26, 27, 28]. It has been suggested that this interaction represents the essential activity of DNA Polε in replication origin firing [25].

The precise molecular mechanism underpinning how the metazoan TopBP1$^{\text{Dpb11}}$, Treslin/$^{\text{Sld3}}$ and MTBP$^{\text{Sld7}}$ deliver GINS and Cdc45 to the Mcm2-7 helicase remains unclear. TopBP1$^{\text{Dpb11}}$ is a multi-BRCT domain scaffold protein containing nine BRCT domains [29]. The triple-BRCT module at the N-terminus of TopBP1$^{\text{Dpb11}}$ plus the BRCT4/5 pair share homology with budding yeast Dpb11 (Fig. 1a(i)) [30]. As Dpb11, TopBP1 facilitates the coupling of origin firing to the cell cycle using its N-terminal BRCT modules [21, 22, 31]. TopBP1$^{\text{Dpb11}}$-BRCT4/5 was, however, found to be non-essential to replication in *Xenopus* egg extracts [31]; perhaps surprisingly as the equivalent BRCT module of Dpb11$^{\text{TopBP1}}$ (BRCT3/4) is essential [23]. The minimal fragment of TopBP1$^{\text{Dpb11}}$ that supports replication includes BRCT0/1/2, BRCT3 (not conserved in Dpb11) and a short segment C-terminal to BRCT3 termed the GINS interaction or GINI region [31, 32]. Yeast-two hybrid experiments showed that the GINI regions of TopBP1 and Dpb11, which have little sequence identity, both bind to GINS [32] (Fig. 1a(i)). As both TopBP1 and Dpb11 are limiting factors for origin firing [33, 34, 35], it is likely that they are released and recycled to facilitate replication from multiple different origins [36]. Both association and disassociation of Dbp11$^{\text{TopBP1}}$ are therefore important processes.
Recent evidence showed that TopBP1$^{\text{Dpb11}}$ and GINS are members of a metazoan pre-LC-like complex that also contains DNA polε and a new metazoa-specific origin firing factor, DONSON [37, 38, 39, 40, 41]. Pre-LC integrity appears to be important for metazoan origin firing because the interactions of DONSON with TopBP1 (via the essential TopBP1-BRCT3 domain), GINS and Mcm3 are necessary for efficient origin firing. The TopBP1-GINS interaction was not characterised in detail in these recent publications.

Here, we have used purified proteins to address how TopBP1 loads GINS onto MCM-DHs to activate the Mcm2-7 helicase during replication origin firing. Our structural, biochemical, and functional studies uncover the binding mode of GINS to TopBP1 and reveal a role for the TopBP1-BRCT4 domain in replication, previously thought to be dispensable. Our data provide a model and framework for future investigation of CMG formation through GINS and Cdc45 loading by TopBP1 and the Treslin-MTBP complex. Moreover, our study provides insight how TopBP1 acts at a molecular level. Such detailed understanding of TopBP1 is key to unravelling how this important scaffold protein can integrate its many different cellular roles in chromosome biology [29].

Results

TopBP1 interacts with GINS *in vivo* and *in vitro*

As previous yeast two-hybrid experiments showed an interaction of the human and *Xenopus* TopBP1-GINI region with GINS (Psf1 and Psf3) [32], we tested if a similar interaction could be detected in human cells. Three proximity biotinylation experiments using cells expressing APEX2-tagged TopBP1 resulted in a specific enrichment of Psf3 upon streptavidin pulldown and mass spectrometry, amongst a range of other known TopBP1 interactors (Supplementary Fig. 2a). Psf2 was also detected in one experiment. Immunoprecipitation from lysates of cells transfected with TopBP1-BRCT0-5 (aa, amino acids 1-766) showed a weak but specific signal for the GINS subunit Sld5 (Supplementary Fig. 2b,c). These experiments suggest that TopBP1 and GINS interact in human cells.

In addition, purified recombinant TopBP1-BRCT0-5 (TopBP1-0-5-WT) co-eluted with the GINS complex from a size exclusion (Fig. 1b; Supplementary Fig. 3a). These results demonstrate that a TopBP1 fragment spanning the BRCT repeats 0-5 is sufficient to interact with GINS both *in vivo* and *in vitro*.

Two binding motifs within TopBP1 contribute to GINS binding

We then used deletion and mutation analysis to narrow down the GINS binding region within the TopBP1-BRCT0-5 fragment. Removing the Treslin-binding BRCT0-2 module (TopBP1-ΔBRCT0/1/2) or BRCT3 (TopBP1-ΔBRCT3) from TopBP1 (Fig. 1a(ii)) did not affect binding (Supplementary Fig. 3b,c). In contrast, deleting BRCT4/5 downstream of the GINI region (TopBP1-ΔBRCT4/5) strongly impaired GINS interaction (Fig. 1c). We confirmed that the phospho-binding pocket of BRCT5 was not required for this interaction, using a triple point mutant that compromises its phospho-binding ability (B5mut) [42] (Fig 1a(ii), Supplementary Fig. 3d,e)). Our observations strongly suggested that a second GINS-binding motif, in addition to the GINI region, is present in the BRCT4/5 module. This was interesting, as no replication role for TopBP1-BRCT4/5 had been defined previously.

Cryo-EM structure of TopBP1-BRCT4/5 in complex with GINS

To reveal how TopBP1 interacts with the GINS complex, peak fractions of TopBP1-BRCTΔ0/1/2 in complex with GINS eluting from the size exclusion column (Supplementary

166 Fig. 3b) were used for cryo-EM. Movies were collected on an FEI Titan Krios microscope
167 equipped with a Gatan K3 camera. 18,945 movies were processed using a combination of
168 CryoSPARC [43] and RELION [44] (Supplementary Fig. 4, Supplementary Table 1) to produce a
169 final 3-dimensional reconstruction, derived from 208,115 particles at 4.6 Å based on Fourier
170 shell correlation (FSC) values. Density corresponding to the GINS tetramer could be readily
171 identified in the resultant map, allowing facile placement of an X-ray crystal structure by rigid-
172 body docking (PDB:2E9X) (Fig. 2a). As features of the individual GINS subunits were clearly
173 identifiable, this also allowed unambiguous orientation of the pseudo-symmetric complex. The
174 crystal structure appeared to account for all the density seen with the exception of a protrusion
175 away from the main body of the GINS complex. This remaining density was too large to
176 represent just the B domain of Psf1 (absent from the docked X-ray crystal structure), or the
177 single BRCT3 of TopBP1, but was readily accounted for by docking of the X-ray crystal
178 structure for TopBP1-BRCT4/5 (PDB:3UEN). The two BRCT domains were arranged such
179 that BRCT4 interacted directly with the Psf1 subunit of GINS.
180
181 The GINS interacting region within the BRCT4 repeat of TopBP1 faces towards the A domain
182 of Psf1 and the linker region connecting domains A and B (Fig. 2a,b), close to where the B
183 domain docks to the CMG helicase (B domain not resolved). Note that some ambiguity exists
184 as to the precise molecular details due to the moderate resolution. In BRCT4, the interaction
185 surface involves a region around beta strands β3 and β4. This region diverts from the canonical
186 BRCT fold in that it lacks an alpha helix (α2) [44] as if to create space for GINS binding
187 (Supplementary Fig. 5a,b). The region shows high sequence conservation in BRCT4
188 equivalents across a wide range of metazoans (Supplementary Fig. 5c). The GINS interaction
189 surface in BRCT4 consists of residues found at the edge of the central four-stranded β-sheet,
190 with additional interactions made by residues in the loops connecting the strands, including
191 amino acids in the variant region between strands β3 and β4. Together, TopBP1-BRCT4 binds
192 to the A domain of Psf1 and involves the linker region located towards the B domain. To our
193 knowledge, this represents a novel mode for a BRCT domain-mediated interaction.
194
195 TopBP1 residues Val590, Thr606 and Val610 appeared to be involved in the interface,
196 providing a series of direct hydrophobic interactions with the side chains of Trp92 and Ile97 in
197 Psf1 (Fig. 2b). We mutated the three TopBP1 residues to glutamate, arginine and glutamate,
198 respectively, and tested if the resulting protein (TopBP1-B4mut; Fig. 1a(ii)) co-purified with
199 GINS. Here, TopBP1-B4mut was strongly compromised in its ability to bind GINS (Fig. 2c)
200 but could still interact with phospho-53BP1 (Supplementary Fig. 6a). We also altered the
201 opposing Psf1 interface by mutating Ile97 to an arginine (Psf1-I97R). Recombinant Psf1-I97R
202 bound TopBP1 weaker than the wild type protein (Fig. 2d), but could still form GINS tetramers
203 (Supplementary Fig. 6b).
204
205 **TopBP1 requires the conserved core of the GINI region for GINS binding**
206 As the predicted interface between the TopBP1-GINI region and GINS [32] was not evident in
207 our cryo-EM map we used additional interaction experiments to validate a role for this motif
208 in GINS binding. The GINI region had been loosely defined as sitting between TopBP1-

209 BRCT3 and BRCT4 (Fig. 1a(i)). Multiple sequence alignment across this region revealed a
210 high degree of conservation between vertebrate species with the section from Glu484 to
211 tyrosine 494 consisting of almost completely identical amino acids (Fig. 3a, Supplementary
212 Fig. 7). We mutated this core, and other regions of conservation, to generate the mutants
213 TopBP1-Gcc (GINI centre core), Gcore (GINI core) and RI-III (regions I-III) (Fig. 3a,
214 Supplementary Fig. 7). Pull-down experiments revealed that TopBP1-Gcc and Gcore, but not
215 RI-III, were compromised in GINS interaction (Fig. 3b). Secondary structure prediction and
216 AlphaFold2 models of TopBP1 suggested the presence of a short helix within this core region
217 for some vertebrate species. By mutation of the central leucine-leucine motif to two
218 consecutive prolines to break the helix (TopBP1-Gpp; Fig. 3a) we could show that the
219 interaction with GINS was strongly compromised, with no effect on binding to 53BP1 (Fig 3c,
220 Supplementary Fig. 6a). To test if this helix constituted a GINS-interaction surface, we used
221 fluorescence polarisation (FP). A fluorescently labelled GINI-core peptide (Ala478-Gly497)
222 bound the GINS tetramer with a dissociation constant of K_d of ~8 μM (Fig. 3d). A peptide
223 harbouring the PP mutation failed to bind (Fig. 3d). We therefore concluded that the GINI
224 region is a GINS interaction site in its own right, but with moderate binding affinity.
225
226 **The GINI-core helix binds Psf1 and 3**
227 We next sought to identify the site in GINS that interacts with the TopBP1-GINI region.
228 Structural prediction using AlphaFold2-Multimer suggested that the GINI-core helix interacted
229 with the distal part of the Psf1 A domain (Fig 4a, Supplementary Fig. 8). Moreover, blind
230 molecular docking simulations with the GINI core region (487-DEDLLSQY-494) resulted in
231 the top-10 solutions clustering in the region of the AlphaFold-predicted GINI binding site
232 (Supplementary Fig. 9).
233
234 A BS^3-crosslinking mass spectrometry experiment with purified recombinant TopBP1-GINS
235 also confirmed the predicted proximity of the TopBP1-GINI core helix region (residues 487-
236 494) and the Psf1-A domain. Several GINI-core-proximal residues crosslinked with Psf1-
237 Lys63 and Thr61 (Supplementary Fig. 10a); both crosslinked Psf1 residues are situated at the
238 distal end of the Psf1 A domain (Supplementary Fig. 10b,c). The GINI-core-proximal residues
239 also crosslinked with lysines 74 and 80 of Psf3; each Psf3 residue also being in close proximity
240 to the predicted site of interaction. Given that the GINI-core helix itself contains no lysine
241 residues, our data are consistent with the hypothesis that this helix binds to both the distal
242 region of the Psf1 A domain and the adjacent region of Psf3 (Supplementary Fig. 10 provides
243 a detailed description).
244
245 With all this information in hand, we could improve the resolution of our cryo-EM data, using
246 an alternative GINS-expression construct, which omits the Psf1-B domain, and served to
247 improve detail around the predicted interaction region (Supplementary Fig. 11). The resultant
248 map showed a volume of extra density that allowed a short helical element to be incorporated
249 into our model, consistent with the AlphaFold2-Multimer predictions (Fig. 4b). The
250 hydrophobic side of the amphipathic GINI-core helix can be seen to pack across two helices of
251 the Psf1-A domain, making interactions with the side chains of Leu490 and Leu491 of the
252 GINI region and Val47, Lys51, Ile59, Ile62, Lys63 and His66 of Psf1. Additionally, the side

253 chain of Tyr494 in the GINI region is inserted into a small pocket on the surface of Psf1 formed
254 by Tyr40, Asn43 and Leu69 with the hydroxyl group picking up a hydrogen bond with the side
255 chain of His66.
256
257 For validation, we mutated Asn43 and Lys51, to Ala and Glu, respectively. Asn43 forms part
258 of the pocket accepting Tyr494 from the GINI region, whilst Lys51 is positioned such that it
259 could form a salt bridge with either Asp487 or Glu495 and part of the hydrophobic grove that
260 accommodates the leucines of the GINI-core helix. Psf1-N43A/K51E readily formed the GINS
261 tetramer (Supplementary Fig. 6b) but was severely compromised in its ability to interact with
262 TopBP1-BRCT0-5-WT (Fig. 4c), again consistent with binding of the GINI region to the distal
263 end of the Psf1-A domain and the adjacent regions in Psf3.
264
265 **Simultaneous inactivation of the GINI core region and BRCT4 is required to suppress**
266 **replication origin firing**
267 Our pulldown interaction studies with GINS and TopBP1-BRCT0-5 carried out at 150 mM
268 sodium chloride suggested that the GINS interacting regions GINI and BRCT4 of TopBP1 are
269 individually required for GINS interaction (Fig. 2c, Fig. 3c). However, pulldowns in sodium
270 acetate revealed specific interactions of the individual interaction regions, albeit at reduced
271 levels compared to TopBP1-WT (Fig 5a, Supplementary Fig. 12a). Here, the GINI region
272 bound to GINS more efficiently than BRCT4. Estimation of binding free energies suggested
273 that the affinities are lower when the surfaces interact individually rather than simultaneously
274 (Fig. 5b). Together, this suggests a model in which both interactions have relatively moderate
275 binding affinities, but cooperate to form a composite interaction surface with high avidity.
276
277 We next asked how the TopBP1-GINI and BRCT4 regions contribute to genome replication,
278 by testing if mutational inactivation of GINI and BRCT4 (Fig. 5c) could suppress replication
279 in *Xenopus* egg extracts. Immunodepleting TopBP1 with two independent antibodies (anti-
280 TopBP1-#1 and #2) effectively removed the endogenous TopBP1 (Fig. 5d(i)), but neither
281 GINS, MTBP, DNA Polε nor Cdc45 (Fig. 5d(ii)), from the extracts. TopBP1 depletion strongly
282 reduced incorporation of radioactive α-^{32}P-dCTP when compared to a mock IgG depletion
283 control (Fig. 5e). Adding recombinant TopBP1-BRCT0-5-WT effectively rescued replication
284 in depleted extracts (Fig. 5e), whereas addition of either TopBP1-BRCT0-5-Gcc or TopBP1-
285 BRCT0-5-Gpp (BRCT4 intact) led to moderately reduced nucleotide incorporation by 21 %
286 and 55 % (120 min time point), respectively (Fig. 5f, Supplementary Fig. 13a), consistent with
287 the observed reduced affinity of BRCT4 for GINS in the absence of a functional GINI region
288 (Fig. 5a, lanes 1-3). TopBP1-ΔBRCT4/5 and TopBP1-B4mut (GINI domain intact) were not
289 detectably compromised in their abilities to support replication (Fig. 5f; Supplementary Fig.
290 13b), as observed before [31, 32], consistent with the GINI region binding GINS stronger than
291 BRCT4 (Fig. 5a, lanes 2,4; Supplementary Fig. 12a). Combination of BRCT4/5 deletion or
292 mutation (B4mut) with either TopBP1-BRCT0-5-Gcc or -Gpp decreased replication to nearly
293 background levels (Fig. 5f, Supplementary Fig. 13), consistent with these double mutants
294 eliminating GINS binding (Fig. 5a, lanes 5, 6; Supplementary Fig. 12a). These results indicate
295 that both TopBP1 binding regions, GINI and BRCT4, are individually capable of supporting

296 replication, whilst simultaneous inactivation of the GINS binding regions strongly suppresses
297 replication.
298
299 We next tested if the TopBP1-GINS interaction is required for replication origin firing. We
300 isolated chromatin from *Xenopus* egg extracts upon TopBP1 immuno-depletion and add-back
301 of TopBP1-BRCT0-5-WT or mutants, 75 minutes after starting replication (a time point when
302 genome replication has progressed significantly). To increase signals, we added aphidicolin,
303 which prevents termination, allowing replisomes to accumulate on chromatin. Mass
304 spectrometry using the CHROMASS protocol [45] and immunoblotting showed chromatin
305 binding of Mcm2-7 subunits in TopBP1-depleted egg extract (Fig. 6a,c,d, Supplementary Fig.
306 14). Addition of geminin, an inhibitor of origin licensing [46], prevented Mcm2-7 binding (Fig.
307 6a,c,d). Together, this confirmed that origin licensing is independent of TopBP1. Several
308 replisome markers, including GINS and Cdc45, were detected on chromatin in TopBP1-
309 depleted extracts containing TopBP1-WT, but were significantly reduced when the TopBP1-
310 Gcc-ΔBRCT4/5 mutant or buffer were added (Fig. 6a,b,d). Thus, the GINS binding sites in
311 TopBP1 are required for origin firing (replisome formation), more precisely for a step between
312 MCM-DH formation and CMG formation. Chromatin samples upon complementation with the
313 single mutant TopBP1-Gcc increased the levels of individual replisome markers weakly but
314 detectably over geminin controls (PolE2 in Fig 6d and Cdc45 in Supplementary Fig. 12b), The
315 TopBP1-ΔBRCT4/5 mutant supported strong replisome formation with only mild effect on
316 Sld5, PCNA, PolE2 and Cdc45 compared to WT (Fig. 6d, lanes 2,5; Supplementary Fig. 12b).
317 Together, this analysis showed that both binding sites are individually capable of supporting
318 origin firing. They do so to different degrees, consistent with the GINI domain mediating
319 stronger GINS interaction than BRCT4. Together, we conclude that both GINS binding sites
320 in TopBP1 act in concert to assemble the CMG helicase. We noticed a surprisingly strong
321 origin firing defect with the TopBP1-Gcc mutant, given that it supports replication to a
322 significant level. It is feasible that compensatory fork acceleration partially compensates for
323 decreased replisome numbers in the Gcc mutant. Our observation that deleting BRCT4 has
324 only minor effects on replisome formation is also consistent with the scenario that the BRCT4-
325 GINS interaction has a role downstream of origin firing that aggravates the DNA synthesis
326 defects (Fig. 5f, Fig. S13) of GINI site mutants.
327
328 **Mutually exclusive binding of TopBP1 and DNA Polε to GINS in the context of CMG**
329 We next explored the relationship between the interactions of TopBP1 and DNA Polε with
330 GINS. These proteins are part of the recently characterised metazoan pre-LC [37, 38, 39, 40].
331 Analysis of pre-LC suggests that GINS may simultaneously bind DNA Polε and TopBP1.
332 When GINS is complexed with DONSON in the pre-LC context, binding sites in Psf1 for the
333 TopBP1-GINI and BRCT4 regions are accessible, as suggested by published Alphafold
334 multimer models [37]. These pre-LC models are less informative on how DNA Polε affects the
335 TopBP1-GINS interaction. The N-terminal region of PolE2 (PolE2-N; aa 1-75) binds GINS
336 mainly at the Psf1-B domain, with minor interactions with residues in the A-domain that partly
337 overlap with the TopBP1-BRCT4 interaction surface (Fig. 7a-c). To test if the Psf1-B domain
338 is required for TopBP1 interaction, we did pulldowns with GINS lacking the Psf1-B domain

339 (Psf1-ΔB). These indicated that the Psf1-B domain is dispensable for interaction with TopBP1-
340 WT (Supplementary Fig. 15a(i)). This could be due a residual affinity of BRCT4 for Psf1-ΔB
341 or due to the GINI-Psf1 interaction. We therefore analysed specifically the interaction of GINS
342 with BRCT4 using the TopBP1-Gcc mutant. TopBP1-Gcc bound to GINS partially
343 dependently on the Psf1-B domain, whereas the B domain had no influence on TopBP1-WT
344 and B4mut binding (Supplementary Fig. 15a(ii)). The moderate effect of the B domain deletion
345 on BRCT4 binding is consistent with the partial overlap of the BRCT4 and PolE2 binding sites
346 in Psf1. Consistently, TopBP1-Gcc, but neither TopBP1-WT nor B4mut, was partially
347 competed off of immobilised GINS by ten times molar excess of PolE2-N (Supplementary Fig.
348 15b(ii)). TopBP1-WT was largely resistant to PolE2 competition also in stringent pulldown
349 conditions (Supplementary Fig. 15b(i). Together, in pre-LC, TopBP1 likely binds GINS
350 through the GINI region, potentially also involving a residual affinity of BRCT4 for GINS
351 despite the presence of DNA Polε. TopBP1 and GINS are likely further stabilised in pre-LCs
352 via their interactions with DONSON [37, 38, 41].
353 Next, we analysed the CMGE helicase. Both TopBP1 binding sites in GINS are accessible in
354 the CMG helicase, showing that TopBP1 could bind in the CMG context (Fig. 7a,b) [27].
355 However, the binding of DNA Polε and TopBP1 seem mutually exclusive. Superposition of
356 CMGE and CMG-TopBP1 revealed potential major steric clashes between TopBP1 and PolE2
357 around the BRCT4 interaction region (Fig. 7a-c). Based on this steric exclusion and the
358 observed direct competition between PolE2 and BRCT4, we propose that TopBP1-BRCT4
359 disengages before DNA Polε associates to form CMGE. Because both TopBP1-GINS binding
360 surfaces must cooperate for a strong GINS interaction BRCT4 disengagement should
361 significantly weaken the TopBP1-GINS complex. Subsequent full dissociation of TopBP1
362 from CMGE may additionally require mechanisms that dislodge DONSON and Treslin-MTBP
363 from CMGE.
364
365 The transition of GINS from TopBP1-bound to a stable CMG requires reconfiguration of the
366 Psf1-B domain [47]. In CMG, the Psf1-B domain adopts a discrete conformation tightly packing
367 against Cdc45 (Fig. 7a) [27]. In contrast, the B domain appears flexible in the GINS tetramer and
368 in the TopBP1-GINS complex, because our cryo-EM data did not detect the B domain at the
369 same map contour level as the rest of GINS (Supplementary Fig. 16a,b). A previous
370 crystallization study of the GINS tetramer also suggested Psf1-B domain flexibility [48]. Thus,
371 integration of GINS in the CMG appears to order the B domain. In this conformation, the B
372 domain binds to the N-terminus of PolE2 once DNA Polε associates to form CMGE [27].
373
374 Together, we envision that the Psf1-B domain reconfigures into a well-ordered state upon CMG
375 assembly. TopBP1-BRCT4 must then dissociate to exchange with DNA Polε for CMGE
376 formation, which likely helps TopBP1 dissociate. Once CMG has formed, DNA Polε seems to
377 dynamically associate with CMG [25]. These observations suggest that the three processes 1)
378 handover of GINS from TopBP1 to MCM-DHs, 2) DNA Polε association and 3) TopBP1
379 dissociation may be mechanistically intertwined.
380
381

382 **Discussion**

383

384 Our data provide an understanding of the interaction between TopBP1^{Dpb11} and GINS at the
385 molecular level, and how this supports replication origin firing. In the past decade, insight into
386 origin firing has largely come from studies focussed on understanding how the yeast Mcm2-7
387 helicase operates as a molecular machine to build replication forks [6, 10, 11, 12, 14, 16, 17, 19, 49, 50, 51,
388 52]. Most recently, the aspect of how GINS and Cdc45 are loaded to activate the helicase through
389 formation of the CMG complex has been addressed in more detail by describing the metazoan
390 pre-LC [37, 38, 39, 40, 41]. Our studies here reveal an important aspect of pre-LC, the essential role
391 of the TopBP1^{Dpb11}-GINS interaction (Supplementary Fig. 17).
392 Formation of the CMG complex serves as a key regulatory step of origin firing. In metazoa
393 and yeast, CMG formation involves the factors Treslin/Sld3, MTBP/Sld7,
394 RecQL4/DONSON/Sld2, TopBP1/Dpb11 and the Mcm2-7 helicase itself. Apart from coupling
395 origin firing to the S phase via S-CDK and DDK, these signal integrators are targeted by the
396 DNA damage checkpoint and other regulatory pathways to mediate DNA damage-dependent
397 origin firing control, execution of the temporal replication program and fine-tuning of origin
398 firing [53, 54, 55, 56, 57, 58, 59, 60, 61, 62, 63, 64, 65, 66, 67]. Such regulation helps avoid replication stress that
399 is key to structural and numerical chromosomal instability in cancer cells [68].

400

401 TopBP1^{Dpb11} is a scaffold protein. To mediate S phase coupling of origin firing, the N-terminal
402 triple BRCT0-2 module of TopBP1^{Dpb11} binds Treslin^{Sld3}, in a strictly phospho-dependant
403 manner, via two CDK sites that are also conserved in budding yeast Sld3^{Treslin} [21, 22]. Despite
404 this level of conservation, some aspects of origin firing in vertebrates are likely to have changed
405 mechanistically when compared to the yeast paradigm: 1) DDK strengthens the interaction
406 between TopBP1^{Dpb11} and the Treslin-MTBP$^{Sld3\text{-}Sld7}$ complex, albeit via an unclarified
407 mechanism [69], whereas a similar role for DDK in yeast has not been reported. 2) an N-terminal
408 fragment that excludes the BRCT4/5 module of TopBP1^{Dpb11} effectively supports replication
409 in *Xenopus* egg extracts [31, 32], whereas the equivalent BRCT3/4 module of Dpb11^{TopBP1} is
410 essential, through CDK-mediated binding to phospho-Sld2$^{RecQL4/DONSON}$ [23]. The metazoan-
411 specific DONSON protein may replace some roles of Sld2 [37, 38, 39, 40]. These mechanistic
412 differences exemplify evolutionary flexibility in S-phase coupling, supported by findings in
413 the *C. elegans* and fission yeast model organisms where the contributions of Treslin^{Sld3} and
414 RecQL4^{Sld2} equivalents have changed during evolution [70, 71]. Such flexibility may be supported
415 by the partially redundant roles of S phase kinases (S-CDK and DDK) and their substrates
416 (Treslin^{Sld3}, RecQL4^{Sld2}, Mcm2-7).
417 TopBP1^{Dpb11} supports CMG formation via an interaction with the GINS complex. In budding
418 yeast, Dpb11^{TopBP1} and GINS are recruited to MCM-DHs as part of a pre-loading complex (pre-
419 LC) comprising Dpb11^{TopBP1}, GINS, DNA Polε and Sld2$^{RecQL4/DONSON}$ [72]. Dpb11^{TopBP1} appears
420 to dock the pre-LC onto Sld3^{Treslin}-Sld7^{MTBP}-Cdc45 via the CDK-mediated Dpb11^{TopBP1}-
421 Sld3^{Treslin} interaction; DDK is required for initial binding of Sld3^{Treslin}-Sld7^{MTBP}-Cdc45 onto
422 MCM-DHs [14, 19]. In metazoans, RecQL4^{Sld2} is not part of the stable protein complex defined as
423 pre-LC, which instead contains DONSON. DONSON is a scaffold protein with a series of
424 interaction sites for TopBP1^{Dpb11}, GINS, DNA Polε and Mcm3 (Supplementary Fig. 17a) [37, 38,

425 [39, 40]. Our described TopBP1^{Dpb11}-GINS interaction probably plays a role in the context of pre-
426 LCs.
427
428 The GINI region of TopBP1^{Dpb11} that had been broadly defined as the region between BRCT3
429 and BRCT4, bound to Psf1 and 3 in Y2H experiments [32]. We show here that a short alpha-helix
430 found at the core of the conserved GINI region (GINI-core helix) forms an essential part of the
431 binding surface that is necessary and sufficient for detectable interaction with GINS. This helix
432 cooperates with a second binding site situated in BRCT4 to form a composite high-affinity
433 GINS-interaction surface; involving a hereinto unknown mode of BRCT-interaction that relies
434 on a specific type of BRCT fold found in TopBP1-BRCT4, which lacks helix 2. Notably, our
435 *in vitro* experiments show that each individual GINS interaction site is capable of binding
436 GINS, albeit with reduced efficiency compared to the complete composite interaction surface.
437 This was consistent with the two GINS binding sites being able to support significant levels of
438 replication in *Xenopus* egg extracts, which is in line with an earlier study focussing on the GINI
439 region [32]. These results indicate that even a low affinity TopBP1^{Dpb11}-GINS interaction is
440 sufficient to allow origin firing. *In vivo*, contacts between other pre-LC components may
441 compensate for a weak TopBP1^{Dpb11}-GINS interaction. A high degree of inter-dependence
442 between association of the components was also observed for the yeast pre-LC complex [72].
443 Simultaneous mutation of both GINS binding domains in TopBP1 suppressed origin firing.
444 This suggests that neither interaction site has a unique molecular role beyond GINS binding.
445 The simplest scenario is that their common essential molecular role is to bind GINS
446 chaperoning it onto MCM-DHs.
447 An alternative interpretation of our TopBP1 mutant analysis seems feasible: TopBP1-Δ4/5 and
448 B4mut only resulted in no DNA synthesis defect and a weak origin firing defect. This scenario
449 is consistent with the possibility that the BRCT4-GINS interaction plays an unidentified role
450 in replication, for example in elongation, which could contribute to the observed effect that
451 BRCT4 inactivating mutants aggravate the defects of GINI site mutants in DNA replication
452 assays (nucleotide incorporation).
453
454 Consistent with published Y2H experiments [32], our structural data indicate that the GINI core
455 helix region interacts with both Psf1 and Psf3, at a position close to the distal end of the Psf1
456 A domain, whereas BRCT4 interacts with both the base of the Psf1-A domain and the linker
457 that connects it to the B domain. Notably, the two receiving interfaces in GINS are fully
458 accessible both in the free GINS tetramer and in the CMG context, consistent with a model
459 where TopBP1^{Dpb11} recruits GINS using both motifs (Supplementary Fig. 17b). TopBP1^{Dpb11}
460 may simultaneously bind phosphorylated Treslin^{Sld3}-MTBP^{Sld7} via its N-terminal BRCT0-2
461 module [21, 22, 73], with Treslin^{Sld3} bringing Cdc45 along through its Sld3-Treslin homology
462 domain [18, 74]. One open question in the field had been the biological role of the BRCT3 domain
463 in TopBP1, which has no equivalent in Dpb11. We now know that an essential role of BRCT3
464 is the binding to DONSON [37, 38].
465
466 After delivery of GINS and Cdc45 to form CMG, the subsequent release of pre-LC components
467 including and of Treslin^{Sld3}-MTBP^{Sld7} is likely to be important. Whether DNA Polε is

468 transferred from pre-LC to CMG to form CMGE during pre-LC dissociation is an interesting
469 aspect. Release may help recycle these limiting factors to allow their use to fire late or dormant
470 origins [35]. Moreover, their release from CMG may be essential for converting CMGs into
471 replisomes. If release is essential, these firing factors constitute a firing-inhibitory intermediate
472 as long as they are CMG-bound, and their controlled dissociation could be part of regulating
473 origin firing. Dissociation could be triggered by the Mcm10 and RecQL4 firing factors that
474 have roles downstream of CMG formation, or by CMG binding replisome factors like DNA
475 polymerase alpha.
476 Dissociation and disassembly of Treslin^{Sld3}-MTBP^{Sld7}-TopBP1^{Dpb11} may involve the action of
477 phosphatases to counteract cell cycle kinase phosphorylation [36, 69, 75]. Moreover, the low
478 affinities of the two individual GINS-interacting sites in TopBP1^{Dpb11} offer the idea that release
479 of one site would significantly destabilise the TopBP1-GINS complex to trigger TopBP1^{Dpb11}
480 dissociation. Competition of DNA Polε with TopBP1 binding may also be involved in TopBP1
481 dissociation, because simultaneous binding of the two proteins to CMG is sterically impossible
482 without significant conformational reconfigurations. Whether TopBP1^{Dpb11} dissociation is a
483 prerequisite for DNA Polε association, or whether the polymerase acts to displace TopBP1^{Dpb11}
484 remains unclear. The reconfiguration of the Psf1-B domain during CMG formation suggests
485 another potential mechanism for TopBP1 release. The B domain seems flexible in the TopBP1-
486 GINS complex and establishes an extensive set of interactions with Cdc45 when it reconfigures
487 to form CMG, which might favour Polε binding over TopBP1^{Dpb11}-BRCT4.
488
489 Recent insights have suggested that formation of the CMG complex is tightly associated with
490 (i) splitting of Mcm2-7 double hexamers into single hexamers; (ii) the exchange of ADP for
491 ATP in the Mcm2-7 nucleotide-binding sites; and (iii) limited untwisting of dsDNA inside the
492 central channels [6, 11, 12]. How TopBP1^{Dpb11}, Treslin^{Sld3} and MTBP^{Sld7} relates to these steps will
493 be key to understanding whether their mechanistic roles go beyond just a simple chaperoning
494 function, guiding Cdc45 and GINS to MCM-DHs. For example, the reported homo-
495 dimerization of TopBP1^{Dpb11} and Treslin^{Sld3}-MTBP^{Sld7} and DONSON might play a role in the
496 cooperative conversion of Mcm2-7 hexamers into replisomes, thus guaranteeing bi-directional
497 replication [41, 69, 76].
498
499 Taken together, our data provide insight into, and a testable hypothesis for, the series of
500 molecular events leading to CMG formation, and its regulation; potentially leading to future
501 therapeutic routes for the treatment of cancer, due the high reliance of tumours on high levels
502 of replication initiation [77]. Targeted interference with origin firing could be one potential
503 avenue, consistent with the testing of DDK inhibitors as candidates in clinical trials [78].
504

505 # Methods
506
507
508 **Antibodies**
509

Name	Antigen/source
Anti-DB4	human TopBP1-aa1-360, rabbit, self-made, antigen-purified; working dilution 1/2000 for Western Blots
Anti Sld5	human Sld5-aa1-100, rabbit monoclonal ERP9318, Abcam ab139683; working dilution 1/1000 for Western Blots
Anti-Flag	Flag peptide, mouse, clone M2, Sigma F1804; working dilution 1/1000 for Western Blots
Anti-53BP1	Human 53BP1 aa 350-400, rabbit, Invitrogen PA1-16565; working dilution 1/1000 for Western Blots
Anti-Myc	Myc tag, mouse, clone 9E10; working dilution 1/1000 for Western Blots
Anti-TopBP1 #1	Xenopus TopBP1-aa1-365, rabbit, self-made, antigen-purified; used for immunodepletion only
Anti-TopBP1 #2	Xenopus TopBP1-aa999-1299, rabbit, self-made, antigen-purified; working dilution 1/3000 for Western Blots
Anti-XCdc45	Xenopus Cdc45, rabbit, self-made serum; working dilution 1/1000 for Western Blots
Anti-XSld5	Xenopus Sld5, rabbit, self-made, serum; working dilution 1/1000 for Western Blots
Anti-XPolE2	Xenopus PolE2, rabbit, self-made, serum; working dilution 1/1000 for Western Blots
Anti-Mcm6	Mcm6-aa775-821, rabbit, BETHYL A300-194A; working dilution 1/2000 for Western Blots
Anti-Mcm4	Mcm4-aa750-850, rabbit, Abcam ab4459; working dilution 1/1000 for Western Blots
Anti-PCNA	Human PCNA, mouse, clone PC10; working dilution 1/1000 for Western Blots
Anti-MBP	MBP tag, mouse, New England BioLabs E8032S; working dilution 1/1000 for Western Blots

510
511
512 **DNA plasmids**
513

Plasmid Name	Vector Backbone	Recombinant Protein
BT702	pLib	TopBP1-1-766 L489P/L490P-Strep
BT707	pLib	TopBP1-1-766-Strep
BT708	pLib	TopBP1-1-766 RegionI-Strep
BT709	pLib	TopBP1-1-766 RegionII-Strep
BT710	pLib	TopBP1-1-766 RegionIII-Strep
BT711	pLib	TopBP1-1-766 Gcore-Strep
BT712	pLib	TopBP1-1-766 Gcc-Strep
BT735	pLib	TopBP1-1-766 S654V/K661R/K704E-Strep
BT759	pLib	TopBP1-1-549-Strep

BT760	pLib	TopBP1-1-549 Gcc-Strep
BT761	pLib	TopBP1-1-549-L489P/L490P-Strep
BT770	pLib	TopBP1-1-766 B4mut-Strep
BT772	pLib	TopBP1-1-766Gcc/B4mut-Strep
BT805	pLib	6xHis-3xFlag-Sld5
BT806	pLib	Psf1
BT807	pLib	Psf2
BT808	pLib	Psf3
BT781	pLib	Psf1 N43A/K51E
MD106	pBIG1a	Psf1 Psf2 Psf3 6xHis-3xFlag-Sld5
MD101	pLib	Psf1(1-151)
MD107	pBIG1a	Psf1(1-151) Psf2 Psf3 6xHis-3xFlag-Sld5
MD146	pET17b	HIS-TopBP1-1-766-Strep
MD147	pET17b	HIS-TopBP1-331-766-Strep
BT764	pcDNA5	APEX2-TopBP1
MP784	pcDNA5	TopBP1-APEX2
BT818	pMal	MBP-PolE2-N-1-75 (PolE2-N)

514
515
516 **Protein purification**
517
518 **Purification of recombinant TopBP1**
519 Purification of TopBP1-331-766 (BRCT3-5) for structural studies was done using bacterial
520 expression. BL21(DE3) cells carrying a pET17 plasmid encoding HIS-(3C)-TopBP1-331-766-
521 Strep was were grown in TurboBroth at 37 °C to an OD600 of 2.0 and induced by with 0.5
522 mM IPTG prior to overnight incubation at 16 °C. Lysis by sonication was done in lysis buffer
523 (25 mM HEPES pH 7.5, 200 mM NaCl, 0.5 mM TCEP, 10 U DNASE Turbo and complete,
524 EDTA-free Protease Inhibitor Cocktail (Merck). The resulting lysate was clarified by
525 centrifugation at 40,000 x g for 60 min at 4°C. The supernatant was applied to a 5 ml HiTrap
526 TALON crude column (GE Healthcare, Little Chalfont, UK), washed with lysis buffer,
527 followed by a wash with lysis buffer containing 10 mM imidazole. Elution followed by
528 increasing imidazole to 250 mM. The eluted protein was separated on a 5 ml HiTrap STREP
529 column (GE Healthcare, Little Chalfont, UK), and eluted with 2 mM desthiobiotin. The eluate
530 was concentrated before separation on a Superdex200increase 10 300 column (GE Healthcare,
531 Little Chalfont, UK) equilibrated in 10 mM HEPES pH 7.5, 150 mM NaCl, 0.5 mM TCEP.
532 Recombinant TopBP1-1-766-Strep-WT (BRCT0-5) and mutants for interaction studies and
533 experiments in *Xenopus* egg extract were purified using SF9 insect cells. The cells were grown
534 in suspension in insect cell media (Pan biotech, P04-850 500) at 27°C. Baculoviruses were
535 generated using pLIB-based constructs (Addgene, 80610). 500 ml Sf9 cells ($1x10^6$/ml) were
536 infected with a 1:100 dilution of recombinant baculovirus carrying TopBP1-1-766-Strep-WT
537 or mutants, and were incubated at 27°C for 72 h. Cell pellets were lysed by douncing in 30 ml
538 of lysis buffer (20 mM HEPES pH 8.0, 150 mM NaCl, 0.1% (v/v) Tween-20, 0.5 mM TCEP,
539 protease inhibitor cocktail (Roche Complete protease inhibitor cocktail, 05056489001)). The
540 lysate was centrifuged at 44,800 g for 45 min and the supernatant was loaded onto the
541 StrepTrapHP-1ml column (Cytiva, 28907546). Elution was done using 2.5 mM desthiobiotin

542 in elution buffer (20 mM HEPES pH 8.0, 150 mM NaCl, 0.01% Tween-20 (v/v), 0.5 mM
543 TCEP, 2% (v/v) glycerol, 2.5 mM desthiobiotin).
544
545 **Purification of GINS**
546 **GINS for structural and fluorescence polarisation studies was purified in SF9 insect cells**.
547 Psf2, Psf3 and HIS-(3C)-Sld5 were expressed together with Psf1 or Psf1(1-151; B domain
548 deleted)) from a single baculovirus, respectively, produced using pBig1a. Cell pellets were re-
549 suspended in lysis buffer containing 25 mM HEPES pH 7.5, 200 mM NaCl, 0.5 mM TCEP,
550 10 U DNASE Turbo and complete, EDTA-free Protease Inhibitor Cocktail (Merck), then
551 disrupted by sonication. The resulting lysate was clarified by centrifugation at 40,000 x g for
552 60 min at 4°C. The supernatant was separated on a 5 ml HiTrap TALON crude column (GE
553 Healthcare, Little Chalfont, UK), using washing in lysis buffer supplemented with 10 mM
554 imidazole. Elution was done using a gradient up to 250 mM imidazole. Peak fractions were
555 pooled and concentrated . For subsequent size exclusion chromatography (analytical and for
556 EM) a Superdex200increase 10 300 column (GE Healthcare, Little Chalfont, UK) equilibrated
557 in 10 mM HEPES pH 7.5, 150 mM NaCl, 0.5 mM TCEP was used while for FP experiments
558 a Superdex200 16 600 column (GE Healthcare, Little Chalfont, UK) equilibrated in 25 mM
559 HEPES pH 7.5, 150 mM NaCl, 1 mM EDTA, 0.25 mM TCEP, 0.02 % (v/v) Tween 20 was
560 used.
561 GINS for pulldown experiments was purified using 6xHis-3xFlag-Sld5. Sf9 insect cells in
562 suspension cultures were co-infected with 1:50 dilution of each four recombinant baculoviruses
563 for expressing 6xHis-3xFlag-Sld5, Psf1, Psf2 and Psf3, respectively. The viruses were made
564 using pLib-based plasmids. 72 h post infection, pellets from one litre cells were lysed by
565 douncing in 60 ml of lysis buffer (20 mM HEPES pH 8.0, 300 mM NaCl, 0.1% (v/v) Tween-
566 20, 25 mM imidazole, 0.5 mM TCEP, protease inhibitor cocktail (Roche Complete protease
567 inhibitor cocktail, 05056489001)). The lysate was centrifuged at 44,800 g for 45 min and the
568 supernatant was incubated with 2.5 ml Ni-NTA agarose beads (Qiagen,30210) for 1 h at 4°C.
569 The bound protein was eluted with six bead volumes elution buffer (20 mM HEPES pH 8.0,
570 300 mM NaCl, 0.01% (v/v) Tween-20, 250 mM imidazole, 0.5 mM TCEP, 2% (v/v) glycerol).
571 The eluate was dialysed into 20 mM HEPES pH 8.0, 150 mM NaCl, 0.01% (v/v) Tween-20,
572 0.5 mM TCEP, 2% (v/v) glycerol, and then applied onto an HiTrap HP Q column (Cytiva,
573 17115301). To elute the bound protein, a linear gradient of NaCl (from 150 mM to 1 M) in
574 elution buffer (20 mM HEPES pH8.0, 0.01% (v/v) Tween-20, 0.5mM TCEP, 2% (v/v)
575 glycerol) was applied. Peak fractions were pooled and separated by size exclusion
576 chromatography (equilibration buffer: 20 mM HEPES pH8.0, 300mM NaCl, 0.01% (v/v)
577 Tween-20, 0.5mM TCEP, 2% (v/v) glycerol).
578
579 **Purification of PolE2-N and geminin from *E.coli***
580 PolE2-N-1-75 (amino acids 1-75) with N-terminal MBP-TEV2 tag in pMal, and GST tagged
581 *Xenopus* geminin (Xgeminin) in pGEX were expressed in Rosetta *E. coli* culture. Expressions
582 were induced with 1 mM IPTG at OD600 = 0.6 at 20 °C (PolE2-N) or 25 °C (Xgeminin)
583 overnight. Cells were harvested by centrifugation. For PolE2-N, cell pellets were resuspended
584 in lysis buffer (20 mM Hepes pH 8.0, 150 mM NaCl, 0.5 mM TCEP, 2 % (v/v) glycerol and
585 protease inhibitor cocktail (Roche Complete protease inhibitor cocktail, 05056489001)) and

586 lysed by sonication. The cell lysate was clarified by centrifugation. The supernatant was
587 incubated with amylose resin (New England Biolabs, E8021S) for 1 h before elution with lysis
588 buffer + 10 mM maltose. The peak fraction was dialysed into TopBP1 buffer (20 mM HEPES
589 pH 8.0, 150 mM NaCl, 0.5 mM TCEP, 0.01 % (v/v) Tween20 and 2 % (v/v) glycerol). For
590 Xgeminin, lysis by sonication was carried out in 5 mg/ ml lysozyme, 20 mM Hepes pH 7.7,
591 200 mM NaCl, 5 mM β-mercaptoethanol, 5 % glycerin. After a clarifying centrifugation step,
592 the supernatant was incubated with glutathione-sepharose (0.5 ml per liter culture; GE
593 Healthcare 17513201) for 3 h before elution with lysis buffer + 50 mM glutathione (Applichem
594 A2084,0025). Peak fractions were pooled and dialyzed into XBE2 buffer (100 mM KCl, 2 mM
595 MgCl2, 0.1 mM CaCl2, 1.71 % w:v sucrose, 5 mM K-EGTA, 10 mM HEPES-KOH, pH 7.7)
596 and concentrated to 360 µM Xgeminin. Aliquots were shock frozen and stored at - 80 °C.
597
598 **Size exclusion chromatography for isolating the TopBP1-GINS complex**
599 Recombinant TopBP1 and GINS proteins were mixed in an equimolar ratio to give a final
600 concentration of 20 µM of each component and incubated on ice for at least 30 minutes prior
601 to application to a Superdex200increase 10 300 column (GE Healthcare, Little Chalfont, UK)
602 equilibrated in 10 mM HEPES pH 7.5, 150 mM NaCl, 0.5 mM TCEP.
603
604 **Fluorescence polarisation experiments**
605 Fluorescein-labelled peptides (WT: Flu-GYGAPSEKHEQADEDLLSQYENG or LLPP: Flu-
606 GYGAPSEKHEQADEDPPSQYENG) (Peptide Protein Research Ltd, Bishops Waltham, UK)
607 at a concentration of 100 nM, were incubated at room temperature with increasing
608 concentrations of GINS in 25 mM HEPES pH 7.5, 150 mM NaCl, 1 mM EDTA, 0.25 mM
609 TCEP, 0.02 % (v/v) Tween 20 in a black 96-well polypropylene plate (VWR, Lutterworth,
610 UK). Fluorescence polarisation was measured in a POLARstar Omega multimode microplate
611 reader (BMG Labtech GmbH, Offenburg, Germany). Binding curves represent the mean of
612 three independent experiments, with error bars representing SEM.
613
614 **Immunoprecipitations from transiently transfected 293T cells**
615 Transient transfections of 6xMyc-Tev2-TopBP1 into 293T cells (ATCC CRL-11268) were
616 carried out using PEI (polyethyleneimine) according to a protocol kindly shared by David
617 Cortez' lab. 4 µg plasmid DNA in 100 µl DMEM (Thermofisher, 41965039) without
618 penicillin-streptomycin were combined with 2.4 µl Polyethylenimin (Sigma, 408727; 10
619 mg/ml) and incubated for 20 minutes before addition to 4 x 10^6 cells on a 10 cm dish.
620 Transfected cells were used 72 h post transfection. 72 h post transfection, 293T cells were lysed
621 by douncing in ten times cell pellet volume of lysis buffer (20 mM HEPES pH8.0, 150mM
622 NaCl, 0.1 % (v/v) Tween-20, 0.5mM TCEP, 2% (v/v) glycerol, protease inhibitor cocktail
623 (Roche, Complete protease inhibitor cocktail, 05056489001)), and centrifuged at 20,000 g for
624 15 min at 4 °C. The soluble supernatant was added to magnetic anti-Myc beads (5 µl slurry per
625 sample; Thermofischer, 88842) and incubated for two hours at 4 °C rotating. Cells equivalent
626 to 50 % of a 15 cm dish were used per sample. Beads were washed three times in lysis buffer
627 with 5 min incubation each, and finally boiled in 50 µl Laemmli loading buffer (6.5 % glycerol,
628 715 mM β-mercaptoethanol, 3% SDS, 62.5 mM Tris-HCl pH 7.9, 0.005 % bromphenol blue).
629

630 **Pulldown experiments of recombinant PolE2-N or TopBP1 using immobilised GINS**
631 Magnetic anti-Flag beads (1 µl slurry for western blot/silver staining-scale experiments, 4 µl
632 for Coomassie-scale experiments) were coupled with 600 ng (western/silver-scale) or 2400 ng
633 (coomassie-scale) GINS via 3xFlag-Sld5. 100 nM final concentration of TopBP1-BRCT0-5-
634 Strep (WT or mutants) in 20 µl (western/silver-scale) or 80 µl (coomassie-scale) of interaction
635 buffer (20 mM HEPES pH8.0, 150mM NaCl (or 100 mM NaCH3COO when indicated), 0.01%
636 (v/v) Tween-20, 0.5mM TCEP, 2% (v/v) glycerol) were added to GINS-coupled beads in 5 µl
637 (western/silver-scale) or 20 µl (coomassie-scale) interaction buffer. For PolE2-N, 1 µM PolE2-
638 N protein in 20 µl were used for GINS-coupled beads in 5 µl reaction buffer. After incubation
639 for 45 min at 4°C rotating, beads were washed three times for 5 min with interaction buffer and
640 boiled in 50 µl Laemmli buffer before SDS PAGE.
641
642 **Pulldown from cell lysates with recombinant TopBP1-1-766-strep (BRCT0-5)**
643 For pulldown assays from soluble lysates of non-transfected 293T cells, 5 µl streptactin
644 Sepharose HP (Cytiva, 28935599) beads were coupled with 10 µg recombinant TopBP1-1-
645 766-strep-WT or mutants in coupling buffer (20 mM HEPES pH8.0, 150mM NaCl, 0.1% (v/v)
646 Tween-20, 0.5mM TCEP, 2% (v/v) glycerol) for 45 min at 4 °C before washing two times with
647 coupling buffer and then once in cell lysis buffer (20 mM HEPES pH8.0, 150mM NaCl, 0.1%
648 (v/v) Tween-20, 0.5mM TCEP, 2% (v/v) glycerol, protease inhibitor cocktail (Roche Complete
649 protease inhibitor cocktail, 05056489001). Control pulldowns were done with Flag-peptide-
650 coupled beads or, when indicated, using GINS-coupled beads and the non-GINS binding
651 TopBP1-Gcc-B4mut. 293T cells were lysed in ten times pellet volume of cell lysis buffer, and
652 centrifuged at 20,000 g for 15 min at 4 °C. Soluble lysate from cells equivalent to 50 % of a 15
653 cm tissue culture plate was added to the TopBP1-coupled beads and incubated for 2 h at 4°C
654 rotating. Beads were washed three times with 5 min incubation in lysis buffer and boiled in 50
655 µl Laemmli buffer before SDS PAGE.
656
657 **Generation of replicating *Xenopus* egg extracts**
658 *Xenopus laevis* egg extracts were prepared from metaphase II arrested eggs as described in [79].
659 After washing with MMR (100 mM NaCl, 2 mM KCl, 1 mM $MgCl_2$, 2 mM $CaCl_2$, 0.1 mM
660 EDTA, 5 mM HEPES–NaOH, pH 7.8) eggs were dejellied (2% cysteine w:v in H_2O, pH 7.8
661 with NaOH). Eggs were rinsed in XBE2 (100 mM KCl, 2 mM $MgCl_2$, 0.1 mM $CaCl_2$, 1.71 %
662 w:v sucrose, 5 mM K-EGTA, 10 mM HEPES-KOH, pH 7.7). Then, the eggs were transferred
663 into centrifuge tubes containing 1 ml XBE2 + 10 µg/ ml protease inhibitor (aprotinin Sigma
664 A6279, leupeptin Merck 108975, pepstatin Carl Roth 2936.1) + 100 µg/ ml cytochalasin D
665 (Sigma C8273). For packing, eggs were centrifuged for 1 min at 1,400 g at 16 °C in a swingout
666 rotor. Excess buffer, activated and apoptotic eggs were removed before crushing the eggs at
667 16,000 g for 10 min at 16 °C. The extract was collected with a 20 G needle and supplemented
668 with 10 µg/ml cytochalasin D, 10 µg/ml protease inhibitors, 1:80 dilution of energy regenerator
669 (1M phosphocreatine K salt, 600 µg/ ml creatine phosphokinase in 10 mM HEPES–KOH pH
670 7.6) and LFB1/50 (10% w:v sucrose, 50 mM KCl, 2 mM $MgCl_2$, 1 mM EGTA, 2 mM DTT,
671 20 mM K_2HPO_4/KH_2PO_4 pH 8.0, 40 mM HEPES–KOH, pH 8.0) to 15 % (v:v). The extract
672 was cleared at 84,000 g at 4 °C for 20 min in a swingout rotor. The cytoplasmatic layer was

673 collected and supplemented with 2 % glycerol v:v. The extract was frozen by dropping 20 µl
674 aliquots into liquid nitrogen and stored at - 80 °C.
675
676 **Immunodepletion of TopBP1 from *Xenopus* egg extract:**
677 For XTopBP1 depletion from *Xenopus* egg extract, 0.5 µg antibody #1, #2 or IgG (rabbit; self-
678 made) were coupled per µl magnetic Protein G dynabeads (Life Technologies 10004D) for 1 h
679 at RT. Freshly thawed extracts were supplemented with 1/40 energy regenerator and 250 µg/ml
680 cycloheximide and released into interphase by adding 0.3 mM $CaCl_2$ for 15 min at 23 °C.
681 Subsequently, extracts were depleted for 45 min on ice with 0.675 µg antibody per µl extract.
682 After depletion the extract was aliquoted, snap frozen and stored at - 80 °C for replication
683 assays and chromatin isolations.
684
685 **Xenopus egg extract replication assays**
686 For TopBP1 addback experiments, 6 ng/ µl recombinant TopBP1 protein or buffer were added
687 to TopBP1 immunodepleted interphase *Xenopus* egg extract containing 50 nCi/µl α^{32}P-dCTP
688 (Perkin Elmer NEG513A250UC). To start the replication reaction the egg extracts were
689 supplemented with 5 ng sperm DNA (kindly provided by the lab of O. Stemmann) per µl
690 extract and incubated at 23°C. 1 µl extract was spotted for each time point onto a glass fibre
691 membrane. Unbound α^{32}P-dCTP was removed by rinsing the membrane three times 15 min
692 with ice cold 5 % TCA in water and once with ice cold EtOH. Newly replicated DNA was
693 detected by phospho-imaging. Standard error of the mean was calculated from three
694 independent experiments.
695
696 **Chromatin isolation from *Xenopus* egg extracts and analysis by mass spectrometry**
697 **(CHROMASS) and western blotting**
698 For chromatin isolation, XTopBP1-depleted interphase egg extract was supplemented with 50
699 µg/ml aphidicolin and aliquoted into 15 µl samples before addition of buffer or recombinant
700 TopBP1 to a final concentration 6 ng/µl. 2.25 µM Xgeminin or buffer were added before
701 incubation for 10 min on ice. To start the replication, 9 ng sperm DNA/µl extract was added
702 and incubated for 75 min at 23°C. Reactions were stopped with 300 µl ice cold ELB salt (10
703 mM HEPES-KOH pH 7.7, 50 mM KCl, 2.5 mM $MgCl_2$) + 250 mM sucrose + 0.6 % triton X-
704 100. The diluted extract was loaded onto a sucrose cushion (150 µl ELB salt + 25 % sucrose)
705 and centrifuged for 10 min at 2500 g at 4 °C in a swingout rotor. The supernatant above the
706 sucrose cushion was removed and the cushion surface was washed twice with 200 µl ELB salt
707 containing 250 mM sucrose. The cushion was removed leaving about 15 µl behind, followed
708 by centrifugation for 2 min at 10,000 g at 4 °C in a fixed angle rotor. For western blotting, the
709 chromatin pellet was resuspended in 24 µl 1x Laemmli SDS sample buffer (6.5 % glycerol,
710 715 mM β-mercaptoethanol, 3% SDS, 62.5 mM Tris-HCl pH 7.9, 0.005 % bromphenol blue)
711 and 5 µl were separated by denaturing SDS PAGE. For MS analysis, four biological replicates
712 of chromatin pellets were analysed by CHROMASS [45]. In brief, chromatin pellets were
713 resuspended in 50 µl denaturation buffer (8 M Urea; 100 mM Tris pH 8). Dithiothreitol (DTT)
714 was added to a final concentration of 5 mM and samples were incubated at 22 °C for 30
715 minutes. To alkylate peptides, iodoacetamide (20 mM) was added and samples were incubated
716 at 37 °C for 30 minutes. DTT (25 mM) was added, and samples were incubated at 22 °C for 5

717 minutes. 500 ng Lys-C (add Supplier) were added, and samples were incubated at 37 °C for 3
718 hours. Samples were diluted with 100 mM ammonium bicarbonate to adjust the urea
719 concentration to 1 M. Trypsin (Sigma, 500 ng per sample) was added and samples were
720 incubated over night at 37 °C. Digested peptides were acidified with 1 % trifluoroacetic acid
721 (TFA) and desalted on Empore C18 material according to Rappsilber et al.
722 *https://www.nature.com/articles/nprot.2007.261).* Eluted peptides were dried in a vacuum
723 concentrator and reconstituted with 9 µl of buffer A (0.1% formic acid) containing 0.2%
724 acetonitrile and 0.01% trifluoro acetic acid. For MS analysis, 4 µl of the reconstituted peptides
725 were separated on an EASY-nLC™ 1200 chromatography system (Thermo Scientific) coupled
726 to a Q Exactive HF-X Orbitrap LC-MS/MS System (Thermo Fisher Scientific) via a Nanoflex
727 ion source. Peptide separation was carried out in analytical columns (50 cm, 75 µm inner
728 diameter packed in-house with C18 resin ReproSilPur 120, 1.9 µm diameter Dr. Maisch) using
729 a 3-hour non-linear gradient at a flow rate of 250 nl/minute using buffer A (aqueous 0.1%
730 formic acid) and buffer B (80 % acetonitrile, 0.1% formic acid). MS data was acquired in data-
731 dependent fashion using a Top15 method. The exact parameters for chromatography and MS
732 instrument settings can be retrieved from the raw files available at ProteomeXchange
733 (PXD040024).
734 MS data files from single-shot experiments were processed with MaxQuant (version 2.0.1.0)
735 using a non-redundant *Xenopus laevis* data base available at ProteomExchange (PXD040024)
736 [45]. Raw data were normalized using the label-free quantitation (LFQ) algorithm implemented
737 in MaxQuant. MS Data with Perseus (version 1.6.15.0) [80]. Protein groups were filtered to
738 eliminate contaminants, reverse hits, and proteins identified by site only. For the heat map (Fig.
739 6a) LFQ intensities were log2 transformed and for each protein z-scores were calculated across
740 all replicates (N=4) of all four conditions. Subsequently, the average of the z-scores was
741 calculated for each condition and selected proteins were plotted (see suppl. table 2 for the z-
742 score of all proteins). Proteins were manually annotated and sorted according to their function
743 in DNA replication and DNA repair. To identify proteins with significant abundance changes
744 between the four conditions, LFQ intensities were log2 transformed and missing values were
745 imputed with random values drawn from a normal distribution centred around the detection
746 limit of the MS instrument (Perseus imputation; width=0.3, down shift = 1.8). Two sample
747 Student's t-tests were carried out in Perseus. Student's t-tests were carried out in Perseus. For
748 these tests three valid values in at least one quadruplicate of either of the tested conditions was
749 required. FDR was adjusted for multiple testing by the Benjamini-Hochberg procedure using
750 a significance threshold of FDR<0.05 (see suppl. table 2). Data visualisation was carried out
751 in R. All scripts are available upon request.
752
753 **Determination of TopBP1-proximal proteins by APEX2 biotinylation**
754 *Sample preparation:*
755 Proximity labelling was performed in isogenic stable 293 Flip-In (Thermo Fisher; R75007)
756 cells stably expressing TopBP1 N-terminal tagged with APEX2 or in 293T cells transiently
757 expressing either N-terminal or C-terminally APEX2-tagged TopBP1. 24 h before transfection,
758 0.8 x 10^6 cells were seeded onto a 6 cm plate. For each condition, four dishes were separately
759 transfected (biological replicates). One day after transfection, cells were incubated for 30 min
760 with 500 µM biotin phenol at 37 °C, before incubation for 1 min at RT with or without

761 (controls) 1 mM H_2O_2. The medium was discarded, and cells were washed three times with
762 quenching buffer (10 mM sodium azide, 10 mM sodium ascorbate and 5 mM Trolox in
763 Dulbecco's PBS (Life Technologies 14190169). Cells were rinsed off the dishes with DPBS,
764 transferred into reaction tubes before washing again with DPBS. Cells were lysed at 95 °C for
765 10 min in TSD buffer (50 mM Tris pH 7.5, 5 mM DTT and 1 % SDS). Samples were diluted
766 ten times with TNN buffer (20 mM Tris pH 7.9, 200 mM NaCl and 0.5 % NP-40 alternative)
767 and benzonase (75 U per sample) (Sigma E1014). Samples were incubated for 15 min at 4 °C
768 and centrifuged at 21000 g for 2 min at 4 °C. Supernatants were incubated over night with 15
769 µl streptavidin sepharose beads (Sigma GE17-5113-01) at 4 °C. Beads were washed once with
770 TNN buffer + 0.1% SDS and twice with 25 mM ammonium bicarbonate before processing for
771 mass spectrometry. For this, captured proteins were washed two times with H_2O prior to on-
772 bead digestion to remove MS incompatible buffer components. The beads were taken up in
773 100 µl 0.8 M urea, 50 mM ammonium bicarbonate buffer (ABC) and supplemented with 5 mM
774 DTT. After incubation at 37°C for 30 min, 10 mM iodoacetamide (IAM) was added and
775 incubated for 30 min at room temperature in the dark while shaking at 1500 rpm (Thermomixer
776 C, Eppendorf). The IAM was quenched with 11 mM DTT. Trypsin was added to a total of 300
777 ng Trypsin per sample. The samples were incubated over night at 37°C, shaking at 1150 rpm
778 before stopping by 1% (vol/vol) formic acid (FA). After bead collection by centrifugation (650
779 g, 5 min) 100 µl supernatant were transferred to a Eppendorf Lo-bind 1.5 ml tube. The
780 remaining beads were incubated with 50 µl 1 % formic acid for (1150 rpm, 5 min rpm, RT)
781 and after collecting the beads once more by centrifugation (650 g, 5 min) the supernatant was
782 combined with the first one. The sepharose beads were discarded. To remove residual
783 sepharose beads, the combined peptide containing solutions were passed over pre-equilibrated
784 (50 µl 0.5 % formic acid) home-made 2-disc Glass microfiber StageTip (disc material: GE
785 Healthcare; pore size: 1.2 µM; thickness: 0.26 mm; 50× g 2 min). The cleared tryptic digests
786 were then desalted on home-made C18 StageTips as described [81]. Briefly, peptides were
787 immobilized and washed on a 2 disc C18 (Empore) StageTip. After elution from the StageTips,
788 samples were dried using a vacuum concentrator (Eppendorf) and the peptides were taken up
789 in 0.1% formic acid solution (10-15 µl) and directly used for LC-MS/MS experiments.
790 *LC-MS/MS settings:*
791 MS Experiments were performed on an Orbitrap Fusion LUMOS instrument (Thermo) coupled
792 to an EASY-nLC 1200 ultra-performance liquid chromatography (UPLC) system (Thermo).
793 The UPLC was operated in the one-column mode. The analytical column was a fused silica
794 capillary (75 µm × 46 cm) with an integrated fritted emitter (CoAnn Technologies) packed in-
795 house with Kinetex 1.7 µm C18-XB core shell beads (Phenomenex). The analytical column
796 was encased by a column oven (Sonation PRSO-V2) and attached to a nanospray flex ion
797 source (Thermo). The column oven temperature was set to 50 °C during sample loading and
798 data acquisition. The LC was equipped with two mobile phases: solvent A (0.2% FA, 2%
799 Acetonitrile, ACN, 97.8% H_2O) and solvent B (0.2% FA, 80% ACN, 19.8% H_2O). All solvents
800 were of UPLC grade (Honeywell). Peptides were directly loaded onto the analytical column
801 with a maximum flow rate that would not exceed the set pressure limit of 980 bar (usually
802 around 0.4 – 0.6 µl/min). Peptides were subsequently separated on the analytical column by
803 running a 105 min gradient of solvent A and solvent B (start with 3% B; gradient 3% to 9% B
804 for 6:30 min; gradient 9% to 30% B for 62:30 min; gradient 30% to 50% B for 24:00 min; 50%

805 to 100% B for 2:30 min; 100% for 9:30 min) at a flow rate of 300 nl/min. The mass
806 spectrometer was controlled by the Orbitrap Fusion Lumos Tune Application (version
807 3.3.2782.28) and operated using the Xcalibur software (version 4.3.73.11). The mass
808 spectrometer was set in the positive ion mode. The ionization potential (spray voltage) was set
809 to 2.5 kV. Source fragmentation was turned off. Precursor ion scanning was performed in the
810 Orbitrap analyser (FT; fourier transform mass spectrometer) in the scan range of m/z 370-1500
811 and at a resolution of 240000 with the internal lock mass option turned on (lock mass was
812 445.120025 m/z, polysiloxane) [82]. AGC (automatic gain control) was set to standard and
813 acquisition time to auto. Product ion spectra were recorded in a data dependent fashion in the
814 IT (IT; ion trap mass spectrometer) in a variable scan range (auto setting) and at rapid scan
815 rate. Peptides were analysed using the setting top speed (repeating cycle of full precursor ion
816 scan (AGC target set to 300 %; acquisition time set to auto) followed by dependent MS2 scans
817 for 3 seconds (minimum intensity threshold 4×10^3)). The MS2 precursor ions were isolated
818 using the quadrupole (isolation window 1.6 m/z) and fragmentation was achieved by Higher-
819 energy C-trap dissociation (HCD) (normalized collision mode (stepped setting) and normalized
820 collision energy set to 27, 32, 40 %). During MS2 data acquisition dynamic ion exclusion was
821 set to 20 seconds. Only charge states between 2-7 were considered for fragmentation.
822 *Data processing:*
823 RAW spectra were submitted to an Andromeda [83] search in MaxQuant (v2.0.3.0) using the
824 default settings (Cox & Mann 2008) [84]. Label-free quantification and match-between-runs was
825 activated [85]. The MS/MS spectra data were searched against the Uniprot *H. sapiens* reference
826 database (one protein per gene; UP000005640_9606_OPPG.fasta, 20585 entries, downloaded
827 1/10/2022) and a dedicated database containing the APEX2-myc sequence
828 (ACE_0741_SOI_v01.fasta; 1 entry). All searches included a contaminants database search (as
829 implemented in MaxQuant, 246 entries). The contaminants database contains known MS
830 contaminants and was included to estimate the level of contamination. Andromeda searches
831 allowed oxidation of methionine residues (16 Da) and acetylation of the protein N-terminus
832 (42 Da) as dynamic modifications and the static modification of cysteine (57 Da, alkylation
833 with iodoacetamide). Enzyme specificity was set to Trypsin/P with two missed cleavages
834 allowed. The instrument type in Andromeda searches was set to Orbitrap and the precursor
835 mass tolerance was set to ± 20 ppm (first search) and ± 4.5 ppm (main search). The MS/MS
836 match tolerance was set to ± 0.5 Da. The peptide spectrum match FDR and the protein FDR
837 were set to 0.01 (based on target-decoy approach). Minimum peptide length was 7 aa. For
838 protein quantification unique and razor peptides were allowed. Modified peptides were allowed
839 for quantification. The minimum score for modified peptides was 40. Label-free protein
840 quantification was switched on, and unique and razor peptides were considered for
841 quantification with a minimum ratio count of 2. Retention times were recalibrated based on the
842 built-in nonlinear time-rescaling algorithm. MS/MS identifications were transferred between
843 LC-MS/MS runs with the match-between-runs option in which the maximal match time
844 window was set to 0.7 min and the alignment time window set to 20 min. The quantification is
845 based on the value at maximum of the extracted ion current. At least two quantitation events
846 were required for a quantifiable protein. Further analysis and filtering of the results was done
847 in Perseus v1.6.10.0. [80]. For quantification we combined related biological replicates to
848 categorical groups and investigated only those proteins that were found in at least one

849 categorical group in a minimum of 3 out of 4 biological replicates. Comparison of protein
850 group quantities (relative quantification) between different MS runs is based solely on the
851 LFQ's as calculated by MaxQuant, MaxLFQ algorithm [85]. Statistical evaluation was done by
852 two-sided Student's t-testing (FDR=0.05, S0=0.1)
853
854 **Analysis of the TopBP1-GINS by cross-linking mass spectrometry**
855 *Sample preparation*
856 50 µg (1.15 µg/µl) of each GINS and TopBP1-BRCT0-5-strep (amino acids 1-766) were
857 incubated for 45 min on ice in cross-linking buffer (20mM HEPES pH8.0, 150mM NaCl,
858 0.01% Tween20, 2% Glycerol, 0.5mM TCEP). 600 µM or 2500 µM of BS^3 crosslinker were
859 added and incubated for 30 min at 35 °C shaking. The reaction was stopped by adding
860 ammonium bicarbonate to a final concentration of 100 mM. 90 % of the cross-linked sample
861 was used for mass spectrometry analysis of crosslinks. 10% of the reaction were separated by
862 SDS-PAGE . The coomassie-stained gel was cut in slices above the molecular weight of
863 monomeric TopBP1-BRCT0-5-strep for subsequent mass spectrometry.
864 Sample *processing for mass spectrometry*
865 Sample preparation of crosslinked samples for LC/MS/MS is based on the SP3 protocol [86]. 30
866 µg of protein from each cross-linking sample was taken up in 100 µl 1× SP3 lysis buffer (final
867 concentrations: 5% (wt/vol) SDS; 10 mM TCEP; 200 µl40 mM chloracetamide; 200 mM
868 HEPES pH 8) and heated for 5 min at 90 °C. After cooling the samples to room temperature
869 (on ice) a mix of 150 µg hydrophobic (#65152105050250) and 150 µg hydrophilic
870 (#45152105050250) SeraMag Speed Beads (Cytiva) was added (bead to protein ratio 10 to 1)
871 and gently mixed. Then 100 µL 100% vol/vol Ethanol (EtOH) was added before incubation
872 for 20 min at 24°C shaking vigorously. The beads were collected on a magnet and the
873 supernatant aspirated. The beads were then washed 4 times with 180 µL 80 % EtOH (collection
874 time on the magnet minimum of 4 min). The beads were then finally taken up in 100 µL 25
875 mM ammoniumbicarbonate (ABC) containing 1 µg Trypsin (Protein:Trypsin ratio 30:1). To
876 help bead dissociation, samples were incubated for 5 min in a sonification bath (preheated to
877 37°C). Samples were incubated over night shaking at vigorously. Samples were acidified with
878 formic acid (FA, final 1% vol/vol) before collection on a magnet. The supernatants were
879 transferred to a fresh Eppendorf tube, before removing trace beads using a magnet for 5 min.
880 The tryptic digests were then desalted on home-made C18 StageTips as described [81]. Briefly,
881 peptides were immobilized and washed on a 2 disc C18 StageTip. Samples were then dried
882 using a vacuum concentrator (Eppendorf) and the peptides were taken up in 0.1% formic acid
883 solution (10 µl) and directly used for LC-MS/MS experiments.
884 *LC-MS/MS settings crosslinking mass spectrometry:*
885 MS Experiments were performed on an Orbitrap Fusion LUMOS instrument (Thermo) coupled
886 to an EASY-nLC 1200 ultra-performance liquid chromatography (UPLC) system (Thermo).
887 The UPLC was operated in the one-column mode. The analytical column was a fused silica
888 capillary (75 µm × 41 cm) with an integrated fritted emitter (CoAnn Technologies) packed in-
889 house with Kinetex 1.7 µm C18-XB core shell beads (Phenomenex). The analytical column
890 was encased by a column oven (Sonation PRSO-V2) and attached to a nanospray flex ion
891 source (Thermo). The column oven temperature was set to 50 °C during sample loading and
892 data acquisition. The LC was equipped with two mobile phases: solvent A (0.2% FA, 2%

Acetonitrile, ACN, 97.8% H_2O) and solvent B (0.2% FA, 80% ACN, 19.8% H_2O). All solvents were of UPLC grade (Honeywell). Peptides were directly loaded onto the analytical column with a maximum flow rate that would not exceed the set pressure limit of 980 bar (usually around 0.4 – 0.6 µL/min). Peptides were subsequently separated on the analytical column by running a 70 min gradient of solvent A and solvent B (start with 2% B; gradient 2% to 6% B for 5:00 min; gradient 6% to 25% B for 42:00 min; gradient 25% to 40% B for 15:00 min; 40% to 98% B for 1:00 min; 98% for 7:00 min) at a flow rate of 350 nl/min. The mass spectrometer was controlled by the Orbitrap Fusion Lumos Tune Application (version 3.3.2782.28) and operated using the Xcalibur software (version 4.3.73.11). The mass spectrometer was set in the positive ion mode. The ionization potential (spray voltage) was set to 2.5 kV. Source fragmentation was turned off. Precursor ion scanning was performed in the Orbitrap analyser (FT; fourier transform mass spectrometer) in the scan range of m/z 370-1600 and at a resolution of 120000 with the internal lock mass option turned on (lock mass was 445.120025 m/z, polysiloxane) [82]. AGC (automatic gain control) was set to standard and acquisition time to auto. Product ion spectra were recorded in a data dependent fashion in the FT in a variable scan range (auto setting) and at 15000 resolution. Peptides were analysed using a top speed regime (repeating cycle of full precursor ion scan (AGC target set to standard; acquisition time 200 ms) followed by dependent MS2 scans for 5 seconds (minimum intensity threshold 2×10^4). The MS2 precursor ions were isolated using the quadrupole (isolation window 2.0 m/z) and fragmentation was achieved by Higher-energy C-trap dissociation (HCD) (normalized collision mode set to stepped and normalized collision energy set to 27, 30, 33 %). During MS2 data acquisition dynamic ion exclusion was set to 60 seconds. Only charge states between 3-7 were considered for fragmentation.

Data processing protocol:

The searches for crosslinked peptides were performed with two different search engines: MetaMorpheus (MM) version 0.0.320 [87] and pLink2 version v2.3.9 [88]. Searches were performed on the Thermo RAW files using the database ACE_0704_SOI_plus_con_v01.fasta (244 entries). The database contains the sequences for TopBP1 (1-766), PsfI, PsFII, PsfIII, Sld5 and 239 known contaminating proteins found in MS samples. The peptide spectrum match FDR for MM was 0.01 and for pLink2 0.05 (based on target-decoy approach, decoys are generated by the software). The settings for MetaMorpheus were: crosslinker name = DSS _KSTY (note: DSS and BS^3 have identical crosslinker size); crosslinker type = non-cleavable; crosslinker mass = 138.06808; crosslinker modification site 1 = K; crosslinker modification site 2 = KSTY; protease = trypsin; maximum missed cleavages = 3; minimum peptide length = 5; maximum peptide length = 60; initiator methionine behaviour = Variable; max modification isoforms = 1024; fixed modifications = Carbamidomethyl on C, variable modifications = Oxidation on M; parent mass tolerance(s) = ±10 ppm; product mass tolerance = ±20 ppm. The settings for pLink2 were: crosslinker name = DSS-BS^3-KSTY; crosslinker type = non-cleavable; crosslinker mass = 138.06808; crosslinker modification site 1 = K; crosslinker modification site 2 = KSTY; protease = trypsin; maximum missed cleavages = 3; minimum peptide length = 6; maximum peptide length = 60; fixed modifications = Carbamidomethyl on C, variable modifications = Oxidation on M; parent mass tolerance(s) = ±20 ppm; product mass tolerance = ±20 ppm. The results from both searches were converted to the ProXL XML format using the respective converters (metaMorph2ProxlXML.jar,

937 plink2toProxlXML.jar, follow links on the ProXL website; https://proxl-ms.org/) and uploaded
938 to the ProXL server [89]. Analysis and evaluation of crosslinks was performed on our local ProXL
939 Server. The results from both searches was analysed together.
940
941 **Computational modeling**
942 Locally implemented AlphaFold2-Multimer version 2.2.0 [90] was used to predict the binding
943 interfaces of GINS and TopBP1 using the full-length sequences of each GINS subunit and
944 residues 301-766 of human TopBP1. 5 models were obtained, using 5 seeds per model, by
945 default and ranked with the combined score of ipTM+pTM implemented in AlphaFold2-
946 Multimer [90, 91]. The top ranked model used for figure production and statistical plots were
947 produced using Alphapickle 1.5.4 for the top seed from each model.
948 Blind molecular docking for insight into the GINI binding region used the GINI sequence
949 DEDLLSQY of TopBP1 (residues 487-494) in the servers Cluspro [92] (accessed on
950 13/06/2022), HPEPDOCK [93] (accessed on 13/06/2022), and MDockPeP [94 95, 96] (accessed on
951 13/06/2022) web servers with 200 solutions per server. We further extended, refined, and re-
952 scored the sampling, by generating 10 additional conformations per web server solution (for a
953 total of 6000 solutions) with FlexPepDock [97]. The top-10 best-scored solutions were selected
954 for analysis and visualization.
955 The binding free energies of GINS with BRCT4 and GINI were estimated based on the best
956 scored AlphaFold2 model using the web servers PRODIGY [98] and PPI-Affinity [99]. The region
957 of GINI employed for the estimation comprised residues 481 to 496. Both PRODIGY and PPI-
958 Affinity analyze the residues in the binding interface for free energy estimation. PRODIGY
959 uses a linear amino acid chain model, whilst PPI-Affinity uses a structure-based machine
960 learning algorithm.
961
962 **Cryo-electron microscopy**
963 ***Grid preparation***
964 Quantifoil 1.2/1.3, 300 mesh copper grids (Quantifoil) were glow discharged using a Tergeo
965 Plasma Cleaner (Pie Scientific) with an indirect plasma treatment for 30 seconds. Grids were
966 loaded into a Leica EM GP2 (Leica microsystems) and 3 µl of peak fractions from size
967 exclusion chromatography were diluted to 0.1 mg/ml and applied to the front of the grid, with
968 an additional 0.5 µl buffer applied to the grids rear, before back blotting for 3 seconds and
969 plunging into an ethane propane mix.
970 *Electron microscopy and data processing*
971 For dataset 1, grids were stored in liquid nitrogen prior to imaging at 300 kV on a FEI Titan
972 Krios (Thermo Fisher Scientific) equipped with K3 detector (Gatan). 18945 movies were
973 collected, using data acquisition software EPU (Thermo Fisher Scientific), at a magnification
974 of 105000 and a pixel size of 0.85Å using a total dose of 50 e-/Å2. These were motion corrected
975 in 5x5 patches using MOTIONCOR2 [100] implemented in RELION4.0 [44] before importing into
976 cryoSPARC [43]. Micrographs were CTF corrected prior to blob picking and extraction of an
977 initial set of particles. Subsequent filtering by 2D classification removed most of these leaving
978 a cleaned set of particles that were used to produce 4 initial models. The 2D classes and initial
979 models appeared to have at least two distinct sub populations, one containing just the GINS
980 complex alone and one that also had some additional density. In order to distinguish between

these two sets of particles heterorefinement was performed to split the two groups. The first population of particles containing only the GINS complex were then imported into RELION4.0 before several cycles of 3D classification, to yield a final set of 111455 particles that gave a volume at 5.9 Å resolution used to produce the GINS alone volume used in (Supplementary Fig. 16a). The second group of TOPBP1-GINS particles were used to train a TOPAZ model before implementing further picking using TOPAZ [101]. The resulting particles were again filtered by rounds of 2D classification and heterorefinement before exporting the particles, that appeared to consist of the full TOPBP1-GINS complex, into RELION4.0. Several cycles of 3D classification were then performed with classes appearing to lack the additional density eliminated, to yield a final set of 208115 particles. 3D refinement and post-processing of these gave a volume at 4.71Å resolution into which previously solved crystal structures of the GINS complex (29EX) and the central BRCT4/5 module of TopBP1 (3UEN) could be docked.

For dataset 2, grids were stored in liquid nitrogen prior to imaging at 300 kV on a FEI Titan Krios (Thermo Fisher Scientific) equipped with Fakcon 4i detector (Thermo Fisher Scientific). 8808 movies were collected, using data acquisition software EPU (Thermo Fisher Scientific), at a magnification of 120000 and a pixel size of 0.74Å using a total dose of 39.69 e-/Å2. The same processing schedule was followed as for dataset one to yield a final set of 154278 particles. 3D refinement and post-processing of these gave a volume at 4.1 Å resolution into which the previously solved model could be docked alongside the predicted GINI helix from the AlphaFold2-Multimer model. Minor adjustments to the model were made in Coot before refinement of the final model using PHENIX [102].

Data Presentation

Figure panels for all structural data were produced using ChimeraX-1.3

Data Availability

The mass spectrometry proteomics data for the proximity dependent biotinylation experiments, the cross-linking experiments and the chromatin mass spectrometry (CHROMASS) experiments, all generated in this study, have been deposited to the ProteomeXchange Consortium via the PRIDE[103] partner repository (https://www.ebi.ac.uk/pride/archive/) with the dataset identifiers PXD040000 (PDB experiments), PXD040156 (CL-MS experiments) and PXD040024 (CHROMASS experiments). Cryo-EM maps and refined coordinates generated in this study have been deposited in the EMDB and Protein Databank as EMD-16916 and PDB ID 8OK2 respectively. Published Protein Database entries used in this study: 2E9X [https://doi.org/10.2210/pdb2E9X/pdb] (GINS crystal structure); 7PFO [https://doi.org/10.2210/pdb7PFO/pdb] (core human replisome); 3UEN [https://doi.org/10.2210/pdb3UEN/pdb] (TopBP1-BRCT4/5 crystal structure); 6XTX [https://doi.org/10.2210/pdb6XTX/pdb] (human DNA-bound CMG).

Research animals

We have complied with ethical regulations. The protocol used in this study was approved by the Landesamt für Natur-, Umwelt- und Verbraucherschutz, Nordrhein-Westfalen (81-02.05.40.20.050)

Acknowledgements

We thank Nora Cronin, Rebecca Thompson and Daniel Maskell, Yehuda Halfon, Pascale Schelleberger and Fabienne Beuron for assistance with cryo-EM. We also thank Svenja Heimann and Jenny Bormann for technical assistance with crosslinking and APEX2 mass spectrometry and Ken L. Dreger for our local ProXL server. We further thank Stefan Westermann, Hemmo Meyer and Olaf Stemmann for sharing reagents and expertise on biochemistry and *Xenopus* egg extracts. The lab of D.B. was supported by the SFB1430 (Project-ID 424228829) and RTG1739 of the Deutsche Forschungsgemeinschaft (DFG, German Rersearch Foundation) and the NRW Rückkehrerförderprogramm (state of North-Rhine-Westphalia), the labs of A.W.O and L.H.P. by Cancer Research UK Programme Grants C302/A14532 and C302/A24386, and the lab of M.R. by the FOR2800 research group (DFG). E.S.G. acknowledges funding from the DFG under Germany´s Excellence Strategy (EXC 2033 – 390677874 – RESOLV), the instrumentation program of the DFG (436586093) and CRC1430 (Project-ID 424228829). M.K. and F.K. are grateful for funding by the DFG (DFG, INST 20876/322-1 FUGG and CRC1430).

Author contributions:

M.D. performed cryo-EM and biochemical experiments with assistance by I.A.B.. B.T. performed biochemical binding studies by pulldown, most mutation analyses, some *Xenopus* egg extract experiments, and Colab Alphafold predictions that identified the GINI binding site in GINS. M.P. performed experiments using *Xenopus* egg extracts and proximity biotinylation experiments. A.M. generated many point mutant cDNAs and assisted in experiments by B.T. and M.P. Y.H.A. and E.S.G. performed computational modelling and Alphofol2-multimer predictions and analyses. H.S. performed and analysed cross linking-mass spectrometry under supervision of B.T. and including mass spectrometry by F.K. and M.K. M.R. performed CHROMASS experiments together with M.P.. F.K. and M.K performed mass spectrometry for proximity biotinylation and cross linking experiments. A.O.W, L.H.P, M.D. and D.B. conceptualised and supervised the project. D.B. and M.D. wrote the manuscript. D.B. coordinated the work performed individual revision experiments.

Competing interests:

The authors declare no competing interests

1059 **References**

1060 1. Siddiqui K, On KF, Diffley JF. Regulating DNA replication in eukarya. *Cold Spring Harb*
1061 *Perspect Biol* **5**, (2013).
1062
1063 2. Remus D, Beuron F, Tolun G, Griffith JD, Morris EP, Diffley JFX. Concerted loading of
1064 Mcm2-7 double hexamers around DNA during DNA replication origin licensing. *Cell*
1065 **139**, 719-730 (2009).
1066
1067 3. Evrin C*, et al.* A double-hexameric MCM2-7 complex is loaded onto origin DNA during
1068 licensing of eukaryotic DNA replication. *Proc Natl Acad Sci U S A* **106**, 20240-20245
1069 (2009).
1070
1071 4. Li N*, et al.* Structure of the eukaryotic MCM complex at 3.8 A. *Nature* **524**, 186-191
1072 (2015).
1073
1074 5. Georgescu R*, et al.* Structure of eukaryotic CMG helicase at a replication fork and
1075 implications to replisome architecture and origin initiation. *Proc Natl Acad Sci U S A*
1076 **114**, E697-E706 (2017).
1077
1078 6. Douglas ME, Ali FA, Costa A, Diffley JFX. The mechanism of eukaryotic CMG helicase
1079 activation. *Nature* **555**, 265-268 (2018).
1080
1081 7. Moyer SE, Lewis PW, Botchan MR. Isolation of the Cdc45/Mcm2-7/GINS (CMG)
1082 complex, a candidate for the eukaryotic DNA replication fork helicase. *Proc Natl Acad*
1083 *Sci U S A* **103**, 10236-10241 (2006).
1084
1085 8. Ilves I, Petojevic T, Pesavento JJ, Botchan MR. Activation of the MCM2-7 helicase by
1086 association with Cdc45 and GINS proteins. *Mol Cell* **37**, 247-258 (2010).
1087
1088 9. Costa A*, et al.* DNA binding polarity, dimerization, and ATPase ring remodeling in the
1089 CMG helicase of the eukaryotic replisome. *Elife* **3**, e03273 (2014).
1090
1091 10. Yeeles JT, Deegan TD, Janska A, Early A, Diffley JF. Regulated eukaryotic DNA
1092 replication origin firing with purified proteins. *Nature* **519**, 431-435 (2015).
1093
1094 11. Lewis JS*, et al.* Mechanism of replication origin melting nucleated by CMG helicase
1095 assembly. *Nature* **606**, 1007-1014 (2022).
1096
1097 12. Meagher M, Epling LB, Enemark EJ. DNA translocation mechanism of the MCM
1098 complex and implications for replication initiation. *Nat Commun* **10**, 3117 (2019).
1099
1100 13. Kanemaki M, Labib K. Distinct roles for Sld3 and GINS during establishment and
1101 progression of eukaryotic DNA replication forks. *Embo J* **25**, 1753-1763 (2006).
1102
1103 14. Heller RC, Kang S, Lam WM, Chen S, Chan CS, Bell SP. Eukaryotic Origin-Dependent
1104 DNA Replication In Vitro Reveals Sequential Action of DDK and S-CDK Kinases. *Cell* **146**,
1105 80-91 (2011).

1106
1107 15. Francis LI, Randell JC, Takara TJ, Uchima L, Bell SP. Incorporation into the prereplicative
1108 complex activates the Mcm2-7 helicase for Cdc7-Dbf4 phosphorylation. *Genes Dev* **23**,
1109 643-654 (2009).
1110
1111 16. Greiwe JF*, et al.* Structural mechanism for the selective phosphorylation of DNA-
1112 loaded MCM double hexamers by the Dbf4-dependent kinase. *Nat Struct Mol Biol* **29**,
1113 10-20 (2022).
1114
1115 17. Saleh A*, et al.* The structural basis of Cdc7-Dbf4 kinase dependent targeting and
1116 phosphorylation of the MCM2-7 double hexamer. *Nat Commun* **13**, 2915 (2022).
1117
1118 18. Itou H, Muramatsu S, Shirakihara Y, Araki H. Crystal structure of the homology domain
1119 of the eukaryotic DNA replication proteins Sld3/Treslin. *Structure* **22**, 1341-1347
1120 (2014).
1121
1122 19. Deegan TD, Yeeles JT, Diffley JF. Phosphopeptide binding by Sld3 links Dbf4-dependent
1123 kinase to MCM replicative helicase activation. *EMBO J* **35**, 961-973 (2016).
1124
1125 20. Zegerman P, Diffley JFX. Phosphorylation of Sld2 and Sld3 by cyclin-dependent kinases
1126 promotes DNA replication in budding yeast. *Nature* **445**, 281-285 (2007).
1127
1128 21. Kumagai A, Shevchenko A, Dunphy WG. Direct regulation of Treslin by cyclin-
1129 dependent kinase is essential for the onset of DNA replication. *J Cell Biol* **193**, 995-
1130 1007 (2011).
1131
1132 22. Boos D*, et al.* Regulation of DNA Replication through Sld3-Dpb11 Interaction Is
1133 Conserved from Yeast to Humans. *Curr Biol* **21**, 1152-1157 (2011).
1134
1135 23. Tak YS, Tanaka Y, Endo S, Kamimura Y, Araki H. A CDK-catalysed regulatory
1136 phosphorylation for formation of the DNA replication complex Sld2-Dpb11. *Embo J* **25**,
1137 1987-1996 (2006).
1138
1139 24. Gambus A*, et al.* GINS maintains association of Cdc45 with MCM in replisome
1140 progression complexes at eukaryotic DNA replication forks. *Nat Cell Biol* **8**, 358-366
1141 (2006).
1142
1143 25. Sengupta S, van Deursen F, de Piccoli G, Labib K. Dpb2 integrates the leading-strand
1144 DNA polymerase into the eukaryotic replisome. *Curr Biol* **23**, 543-552 (2013).
1145
1146 26. Goswami P*, et al.* Structure of DNA-CMG-Pol epsilon elucidates the roles of the non-
1147 catalytic polymerase modules in the eukaryotic replisome. *Nat Commun* **9**, 5061
1148 (2018).
1149
1150 27. Jones ML, Baris Y, Taylor MRG, Yeeles JTP. Structure of a human replisome shows the
1151 organisation and interactions of a DNA replication machine. *EMBO J* **40**, e108819
1152 (2021).

28. Xu Z*, et al.* Synergism between CMG helicase and leading strand DNA polymerase at replication fork. *Nat Commun* **14**, 5849 (2023).

29. Day M, Oliver AW, Pearl LH. Phosphorylation-dependent assembly of DNA damage response systems and the central roles of TOPBP1. *DNA Repair (Amst)* **108**, 103232 (2021).

30. Makiniemi M*, et al.* BRCT domain-containing protein TopBP1 functions in DNA replication and damage response. *J Biol Chem* **276**, 30399-30406 (2001).

31. Kumagai A, Shevchenko A, Dunphy WG. Treslin collaborates with TopBP1 in triggering the initiation of DNA replication. *Cell* **140**, 349-359 (2010).

32. Tanaka S, Komeda Y, Umemori T, Kubota Y, Takisawa H, Araki H. Efficient initiation of DNA replication in eukaryotes requires Dpb11/TopBP1-GINS interaction. *Mol Cell Biol* **33**, 2614-2622 (2013).

33. Mantiero D, Mackenzie A, Donaldson A, Zegerman P. Limiting replication initiation factors execute the temporal programme of origin firing in budding yeast. *EMBO J* **30**, 4805-4814 (2011).

34. Tanaka S, Nakato R, Katou Y, Shirahige K, Araki H. Origin association of Sld3, Sld7, and Cdc45 proteins is a key step for determination of origin-firing timing. *Curr Biol* **21**, 2055-2063 (2011).

35. Collart C, Allen GE, Bradshaw CR, Smith JC, Zegerman P. Titration of four replication factors is essential for the Xenopus laevis midblastula transition. *Science* **341**, 893-896 (2013).

36. Jenkinson F, Tan KW, Schopf B, Santos MM, Zegerman P. Dephosphorylation of the pre-initiation complex is critical for origin firing. *Mol Cell* **83**, 12-25 e10 (2023).

37. Lim Y*, et al.* In silico protein interaction screening uncovers DONSON's role in replication initiation. *Science*, eadi3448 (2023).

38. Xia Y*, et al.* DNSN-1 recruits GINS for CMG helicase assembly during DNA replication initiation in Caenorhabditis elegans. *Science*, eadi4932 (2023).

39. Kingsley G*, et al.* DONSON facilitates Cdc45 and GINS chromatin association and is essential for DNA replication initiation. *Nucleic Acids Res*, (2023).

40. Hashimoto Y, Sadano K, Miyata N, Ito H, Tanaka H. Novel role of DONSON in CMG helicase assembly during vertebrate DNA replication initiation. *EMBO J*, e114131 (2023).

1199 41. Cvetkovic MA*, et al.* The structural mechanism of dimeric DONSON in replicative
1200 helicase activation. *Mol Cell*, (2023).
1201
1202 42. Bigot N, Day M, Baldock RA, Watts FZ, Oliver AW, Pearl LH. Phosphorylation-mediated
1203 interactions with TOPBP1 couple 53BP1 and 9-1-1 to control the G1 DNA damage
1204 checkpoint. *Elife* **8**, (2019).
1205
1206 43. Punjani A, Rubinstein JL, Fleet DJ, Brubaker MA. cryoSPARC: algorithms for rapid
1207 unsupervised cryo-EM structure determination. *Nat Methods* **14**, 290-296 (2017).
1208
1209 44. Leung CC*, et al.* Structural insights into recognition of MDC1 by TopBP1 in DNA
1210 replication checkpoint control. *Structure* **21**, 1450-1459 (2013).
1211
1212 45. Raschle M*, et al.* DNA repair. Proteomics reveals dynamic assembly of repair
1213 complexes during bypass of DNA cross-links. *Science* **348**, 1253671 (2015).
1214
1215 46. McGarry TJ, Kirschner MW. Geminin, an inhibitor of DNA replication, is degraded
1216 during mitosis. *Cell* **93**, 1043-1053 (1998).
1217
1218 47. Kamada K, Kubota Y, Arata T, Shindo Y, Hanaoka F. Structure of the human GINS
1219 complex and its assembly and functional interface in replication initiation. *Nat Struct*
1220 *Mol Biol* **14**, 388-396 (2007).
1221
1222 48. Chang YP, Wang G, Bermudez V, Hurwitz J, Chen XS. Crystal structure of the GINS
1223 complex and functional insights into its role in DNA replication. *Proc Natl Acad Sci U S*
1224 *A* **104**, 12685-12690 (2007).
1225
1226 49. De Jesus-Kim L, Friedman LJ, Looke M, Ramsoomair CK, Gelles J, Bell SP. DDK regulates
1227 replication initiation by controlling the multiplicity of Cdc45-GINS binding to Mcm2-7.
1228 *Elife* **10**, (2021).
1229
1230 50. Looke M, Maloney MF, Bell SP. Mcm10 regulates DNA replication elongation by
1231 stimulating the CMG replicative helicase. *Genes Dev* **31**, 291-305 (2017).
1232
1233 51. Douglas ME, Diffley JFX. Recruitment of Mcm10 to Sites of Replication Initiation
1234 Requires Direct Binding to the Minichromosome Maintenance (MCM) Complex. *J Biol*
1235 *Chem* **291**, 5879-5888 (2016).
1236
1237 52. Costa A, Diffley JFX. The Initiation of Eukaryotic DNA Replication. *Annu Rev Biochem*
1238 **91**, 107-131 (2022).
1239
1240 53. Zegerman P, Diffley JFX. Checkpoint-dependent inhibition of DNA replication initiation
1241 by Sld3 and Dbf4 phosphorylation. *Nature* **467**, 474-478 (2010).
1242
1243 54. Lopez-Mosqueda J, Maas NL, Jonsson ZO, Defazio-Eli LG, Wohlschlegel J, Toczyski DP.
1244 Damage-induced phosphorylation of Sld3 is important to block late origin firing.
1245 *Nature* **467**, 479-483 (2010).

1246
1247 55. Natsume T*, et al.* Kinetochores coordinate pericentromeric cohesion and early DNA
1248 replication by Cdc7-Dbf4 kinase recruitment. *Mol Cell* **50**, 661-674 (2013).
1249
1250 56. Reusswig KU, Zimmermann F, Galanti L, Pfander B. Robust Replication Control Is
1251 Generated by Temporal Gaps between Licensing and Firing Phases and Depends on
1252 Degradation of Firing Factor Sld2. *Cell Rep* **17**, 556-569 (2016).
1253
1254 57. Tanaka S. Interaction of replication factor Sld3 and histone acetyl transferase Esa1
1255 alleviates gene silencing and promotes the activation of late and dormant replication
1256 origins. *Genetics* **217**, 1-11 (2021).
1257
1258 58. Sansam CG*, et al.* A mechanism for epigenetic control of DNA replication. *Genes Dev*
1259 **32**, 224-229 (2018).
1260
1261 59. Wittig KA, Sansam CG, Noble TD, Goins D, Sansam CL. The CRL4DTL E3 ligase induces
1262 degradation of the DNA replication initiation factor TICRR/TRESLIN specifically during
1263 S phase. *Nucleic Acids Res* **49**, 10507-10523 (2021).
1264
1265 60. Johnson MC, Can G, Santos MM, Alexander D, Zegerman P. Checkpoint inhibition of
1266 origin firing prevents inappropriate replication outside of S-phase. *Elife* **10**, (2021).
1267
1268 61. Ferreira P*, et al.* MTBP phosphorylation controls DNA replication origin firing. *Sci Rep*
1269 **11**, 4242 (2021).
1270
1271 62. Ciardo D*, et al.* Polo-like kinase 1 (Plk1) regulates DNA replication origin firing and
1272 interacts with Rif1 in Xenopus. *Nucleic Acids Res* **49**, 9851-9869 (2021).
1273
1274 63. Bohly N*, et al.* Increased replication origin firing links replication stress to whole
1275 chromosomal instability in human cancer. *Cell Rep* **41**, 111836 (2022).
1276
1277 64. Toledo LI*, et al.* ATR prohibits replication catastrophe by preventing global exhaustion
1278 of RPA. *Cell* **155**, 1088-1103 (2013).
1279
1280 65. Helmrich A, Ballarino M, Nudler E, Tora L. Transcription-replication encounters,
1281 consequences and genomic instability. *Nat Struct Mol Biol* **20**, 412-418 (2013).
1282
1283 66. Rhind N, Gilbert DM. DNA replication timing. *Cold Spring Harb Perspect Biol* **5**,
1284 a010132 (2013).
1285
1286 67. Boos D, Ferreira P. Origin Firing Regulations to Control Genome Replication Timing.
1287 *Genes (Basel)* **10**, (2019).
1288
1289 68. Burrell RA*, et al.* Replication stress links structural and numerical cancer chromosomal
1290 instability. *Nature* **494**, 492-496 (2013).
1291

69. Volpi I, Gillespie PJ, Chadha GS, Blow JJ. The role of DDK and Treslin-MTBP in coordinating replication licensing and pre-initiation complex formation. *Open Biol* **11**, 210121 (2021).

70. Gaggioli V, Zeiser E, Rivers D, Bradshaw CR, Ahringer J, Zegerman P. CDK phosphorylation of SLD-2 is required for replication initiation and germline development in C. elegans. *J Cell Biol* **204**, 507-522 (2014).

71. Fukuura M, Nagao K, Obuse C, Takahashi TS, Nakagawa T, Masukata H. CDK promotes interactions of Sld3 and Drc1 with Cut5 for initiation of DNA replication in fission yeast. *Mol Biol Cell* **22**, 2620-2633 (2011).

72. Muramatsu S, Hirai K, Tak YS, Kamimura Y, Araki H. CDK-dependent complex formation between replication proteins Dpb11, Sld2, Pol (epsilon}, and GINS in budding yeast. *Genes Dev* **24**, 602-612 (2010).

73. Rappas M, Oliver AW, Pearl LH. Structure and function of the Rad9-binding region of the DNA-damage checkpoint adaptor TopBP1. *Nucleic Acids Res*, (2010).

74. Ferreira P, Sanchez-Pulido L, Marko A, Ponting CP, Boos D. Refining the domain architecture model of the replication origin firing factor Treslin/TICRR. *Life Sci Alliance* **5**, (2022).

75. Chou DM, Petersen P, Walter JC, Walter G. Protein phosphatase 2A regulates binding of Cdc45 to the prereplication complex. *J Biol Chem* **277**, 40520-40527 (2002).

76. Kohler K*, et al.* The Cdk8/19-cyclin C transcription regulator functions in genome replication through metazoan Sld7. *PLoS Biol* **17**, e2006767 (2019).

77. Zimmerman KM, Jones RM, Petermann E, Jeggo PA. Diminished origin-licensing capacity specifically sensitizes tumor cells to replication stress. *Mol Cancer Res* **11**, 370-380 (2013).

78. Rainey MD, Quachthithu H, Gaboriau D, Santocanale C. DNA Replication Dynamics and Cellular Responses to ATP Competitive CDC7 Kinase Inhibitors. *ACS Chem Biol* **12**, 1893-1902 (2017).

79. Gillespie PJ, Gambus A, Blow JJ. Preparation and use of Xenopus egg extracts to study DNA replication and chromatin associated proteins. *Methods* **57**, 203-213 (2012).

80. Tyanova S*, et al.* The Perseus computational platform for comprehensive analysis of (prote)omics data. *Nat Methods* **13**, 731-740 (2016).

81. Rappsilber J, Mann M, Ishihama Y. Protocol for micro-purification, enrichment, pre-fractionation and storage of peptides for proteomics using StageTips. *Nat Protoc* **2**, 1896-1906 (2007).

1339 82. Olsen JV*, et al.* Parts per million mass accuracy on an Orbitrap mass spectrometer via
1340 lock mass injection into a C-trap. *Mol Cell Proteomics* **4**, 2010-2021 (2005).
1341
1342 83. Cox J, Neuhauser N, Michalski A, Scheltema RA, Olsen JV, Mann M. Andromeda: a
1343 peptide search engine integrated into the MaxQuant environment. *J Proteome Res* **10**,
1344 1794-1805 (2011).
1345
1346 84. Cox J, Mann M. MaxQuant enables high peptide identification rates, individualized
1347 p.p.b.-range mass accuracies and proteome-wide protein quantification. *Nat*
1348 *Biotechnol* **26**, 1367-1372 (2008).
1349
1350 85. Cox J, Hein MY, Luber CA, Paron I, Nagaraj N, Mann M. Accurate proteome-wide label-
1351 free quantification by delayed normalization and maximal peptide ratio extraction,
1352 termed MaxLFQ. *Mol Cell Proteomics* **13**, 2513-2526 (2014).
1353
1354 86. Hughes CS, Moggridge S, Muller T, Sorensen PH, Morin GB, Krijgsveld J. Single-pot,
1355 solid-phase-enhanced sample preparation for proteomics experiments. *Nat Protoc* **14**,
1356 68-85 (2019).
1357
1358 87. Lu L*, et al.* Identification of MS-Cleavable and Noncleavable Chemically Cross-Linked
1359 Peptides with MetaMorpheus. *J Proteome Res* **17**, 2370-2376 (2018).
1360
1361 88. Chen ZL*, et al.* A high-speed search engine pLink 2 with systematic evaluation for
1362 proteome-scale identification of cross-linked peptides. *Nat Commun* **10**, 3404 (2019).
1363
1364 89. Riffle M, Jaschob D, Zelter A, Davis TN. ProXL (Protein Cross-Linking Database): A
1365 Platform for Analysis, Visualization, and Sharing of Protein Cross-Linking Mass
1366 Spectrometry Data. *J Proteome Res* **15**, 2863-2870 (2016).
1367
1368 90. Evans R*, et al.* Protein complex prediction with AlphaFold-Multimer. *bioRxiv*,
1369 2021.2010.2004.463034 (2022).
1370
1371 91. Jumper J*, et al.* Highly accurate protein structure prediction with AlphaFold. *Nature*
1372 **596**, 583-589 (2021).
1373
1374 92. Kozakov D*, et al.* The ClusPro web server for protein-protein docking. *Nat Protoc* **12**,
1375 255-278 (2017).
1376
1377 93. Zhou P, Jin B, Li H, Huang SY. HPEPDOCK: a web server for blind peptide-protein
1378 docking based on a hierarchical algorithm. *Nucleic Acids Res* **46**, W443-W450 (2018).
1379
1380 94. Yu C*, et al.* A mechanism for preventing asymmetric histone segregation onto
1381 replicating DNA strands. *Science* **361**, 1386-1389 (2018).
1382
1383 95. Xu X, Yan C, Zou X. MDockPeP: An ab-initio protein-peptide docking server. *J Comput*
1384 *Chem* **39**, 2409-2413 (2018).
1385

96. Yan C, Xu X, Zou X. Fully Blind Docking at the Atomic Level for Protein-Peptide Complex Structure Prediction. *Structure* **24**, 1842-1853 (2016).

97. Raveh B, London N, Schueler-Furman O. Sub-angstrom modeling of complexes between flexible peptides and globular proteins. *Proteins* **78**, 2029-2040 (2010).

98. Xue LC, Rodrigues JP, Kastritis PL, Bonvin AM, Vangone A. PRODIGY: a web server for predicting the binding affinity of protein-protein complexes. *Bioinformatics* **32**, 3676-3678 (2016).

99. Romero-Molina S*, et al.* PPI-Affinity: A Web Tool for the Prediction and Optimization of Protein-Peptide and Protein-Protein Binding Affinity. *J Proteome Res* **21**, 1829-1841 (2022).

100. Zheng SQ, Palovcak E, Armache JP, Verba KA, Cheng Y, Agard DA. MotionCor2: anisotropic correction of beam-induced motion for improved cryo-electron microscopy. *Nat Methods* **14**, 331-332 (2017).

101. Bepler T*, et al.* Positive-unlabeled convolutional neural networks for particle picking in cryo-electron micrographs. *Nat Methods* **16**, 1153-1160 (2019).

102. Liebschner D*, et al.* Macromolecular structure determination using X-rays, neutrons and electrons: recent developments in Phenix. *Acta Crystallogr D Struct Biol* **75**, 861-877 (2019).

103. Vizcaino JA*, et al.* 2016 update of the PRIDE database and its related tools. *Nucleic Acids Res* **44**, D447-456 (2016).

1416 # Figure Legends
1417
1418 **Figure 1: GINS and TopBP1 interact.**
1419
1420 a: (i) Domain model of human (hs) TopBP1, its conservation with BRCT1/2 and 3/4 domains
1421 (grey boxes) of budding yeast Dpb11 (scDpb11). Arrows indicate binding domains with
1422 interacting proteins. (ii) Overview of TopBP1 wild type (WT) and BRCT deletion (Δ) and
1423 point mutants. GINS binding capabilities are labelled in red and green. Numbers, amino acid
1424 position; capital letters indicate amino acid substitutions. Amino acid substitutions of point
1425 mutants in BRCT4 (B4mut) and 5 (B5mut) are coloured orange.
1426
1427 b: Elution profiles of size exclusion chromatography (Superdex200) of individual recombinant
1428 TopBP1-BRCT0-5 protein (grey) and GINS tetramers (green), or of both upon incubation
1429 (blue).
1430
1431 c: Recombinant GINS immobilised on Flag-beads and control beads (Flag peptide-coupled
1432 beads) were used to pull down recombinant TopBP1-0-5-WT or TopBP1-ΔBRCT4/5 (compare
1433 a(ii)). SDS gels were silver stained. kDa specifies molecular weight marker bands. The
1434 experiment was done more than three times with similar results.
1435
1436
1437 **Figure 2: Protein structure of the GINS-TopBP1-BRCT4/5 complex.**
1438 a: Structural model of the GINS-TopBP1-BRCT4/5 complex. Crystal structures of the GINS
1439 subunits (shades of green, yellow), and the central BRCT4/5 domain of TopBP1 (grey) were
1440 docked into the cryo-EM volume shown as transparent volume.
1441
1442 b: Zoom-in of the BRCT4-Psf1 interface. The residues in stick representation appear crucial
1443 for the interface. Mutations to break the interaction are coloured pink (Psf1-I97R) and purple
1444 (TopBP1-B4mut; compare Fig. 1a(ii)).
1445
1446 c: Pulldown of the indicated recombinant TopBP1-BRCT0-5-strep versions (see Fig. 1a(ii)) by
1447 Flag-beads-immobilised recombinant GINS or Flag peptide-coupled control beads. Analysis
1448 was done by immunoblotting. The experiment was done more than three times with similar
1449 results.
1450
1451 d: Pulldown of the indicated recombinant TopBP1-BRCT0-5-WT-strep using immobilised
1452 GINS-WT or GINS carrying a Ile97 to arginine mutation in Psf1.TopBP1-Gcc/B4mut-strep
1453 (Fig. 1a(ii), Fig. 3a) was used as a non-GINS binding control. The experiment was done twice
1454 with similar results.
1455
1456
1457 **Figure 3: The conserved core of the TopBP1-GINI domain is required for a stable**
1458 **interaction with GINS**

1459
1460 a: Domain model and T-COFFEE alignment (one-letter aa code) of TopBP1 proteins from
1461 humans (Q92547) *Xenopus laevis* (Q7ZZY3), *Bos taurus* (A0A3Q1LWE4) and *Rattus*
1462 *norvegicus* (A0A8I6GFZ6). Coloured boxes indicate GINI region mutants in sub-regions I
1463 (blue), II (green) and III (orange), and in the GINI core helix (red) (details in Supplementary
1464 Fig. 7). Amino acid substitutions, names of GINI core region mutations and corresponding
1465 GINS binding capabilities are shown. ., : and * indicate low conservation, high conservation
1466 and identical amino acids, respectively.
1467
1468 b/c: Pulldown of recombinant TopBP1-BRCT0-5-strep-WT or the indicated GINI region
1469 mutants (panel a) by bead-immobilised GINS or Flag peptide-coupled control beads. Analysis
1470 was done by immunoblotting. The experiments were done more than three times with similar
1471 results.
1472
1473 d: Fluorescence polarisation measurements including dissociation constants (kD) calculations
1474 using recombinant GINS tetramer and fluorescently labelled TopBP1-GINI-core peptides (WT
1475 or Gpp (panel a)). For each peptide n=3 independent experiments and data are presented as
1476 mean values +/- SEM.
1477
1478
1479 **Figure 4: The TopBP1-GINI domain interacts with Psf1-A domain.**
1480
1481 a: Structural model of TopBP1-BRCT3-5 complexed to the GINS tetramer predicted using
1482 AlphaFold2-Multimer. All chains are represented as cartoon. The transparent volume
1483 represents the surface of the GINS complex (not cryo-EM density). Of TopBP1, only the GINI
1484 helix (residues 485-496) and BRCT4/5 (residues 551-766), are shown.
1485
1486 b: Left: Cryo-EM volume showing extra helical density ascribed to the GINI helix (grey).
1487 Right: a structural model based on this cryo-EM and an AlphaFold2-Multimer predicted
1488 structure.
1489
1490 c: Pulldown of recombinant TopBP1-BRCT0-5-WT-strep using immobilised GINS-WT or
1491 GINS carrying the indicated Psf1 mutations. TopBP1-BRCT0-5-Gcc/B4mut-strep served as a
1492 non-GINS binding control. Analysis was done by immunoblotting. The experiment was done
1493 twice with similar results.
1494
1495
1496 **Figure 5: Both GINS binding surfaces in TopBP1 cooperate in supporting genome**
1497 **replication.**
1498
1499 a: Immobilized recombinant Flag-GINS or Flag peptide-coupled beads were used to pulldown
1500 the indicated recombinant TopBP1-BRCT0-5-strep versions (Fig. 1a, Fig 3a) using 100 mM
1501 NaAc in the binding buffer. The pulldown was analysed by immunoblotting. The experiment
1502 was done twice with similar results.

1503
1504 b: (i) shows the AlphaFold2-Multimer model of the GINS-TopBP1 complex that was used to
1505 estimate the binding free energy using PPI-Affinity and PRODIGY shown in (ii). Estimations
1506 were done for the binding interfaces involving TopBP1-GINI (blue) and TopBP1-BRCT4
1507 (red), both together and alone.
1508
1509 c: Coomassie-stained SDS PAGE gel of the indicated recombinant TopBP1-BRCT0-5 proteins
1510 (Fig. 1a(ii), Fig. 3a).
1511
1512 d: The indicated relative amounts (100 % - 10 %) of immunodepleted and non-depleted
1513 *Xenopus* egg extracts (Xtract) were analysed by immunoblotting using anti-TopBP1 #2 and
1514 other indicated antibodies. TopBP1 antibodies #1 and #2, or unspecific IgG (mock) were used
1515 for immunodepletions. Ponc, ponceau staining. Error bars, SEM, n=3. The experiments were
1516 done more than three times (i) or twice (ii) with similar results.
1517
1518 e/f: Replication analyses (radioactive nucleotide incorporation) using *Xenopus* egg extracts
1519 immunodepleted with antibodies anti-TopBP1#1, #2 or unspecific IgG (mock). Buffer (buf),
1520 recombinant wild-type (WT) or mutant TopBP1-BRCT0-5-strep (panel c) were added.
1521 Diamonds, values of n=3 independent experiments, Error bars, SEM.
1522
1523
1524 **Figure 6: GINS binding to TopBP1 is required for the origin firing step of replication.**
1525 a-c: Heat map showing the intensity of chromatin-bound proteins recovered from TopBP1
1526 depleted interphase *Xenopus* egg extracts supplemented wildtype or mutant TopBP1
1527 determined by quantitative mass spectrometry. Chromatin was isolated 75 min after sperm
1528 addition. All extracts contained 50 mg/ml aphidicolin and, where indicated, 2.25 mM
1529 geminin. The heat map shows log2 transformed label-free quantification (LFQ) intensities z-
1530 score normalized across rows and mean averaged over four independent replicates (n=4).
1531
1532 b/c) volcano plots highlighting a selection of differentially detected proteins in samples
1533 described in a). Log2 transformed LFQ intensities from four replicates each were analysed by
1534 a two-sided Student's t-test. For clarity, only proteins involved in DNA replication are labelled
1535 (all significantly enriched proteins are labelled in Supplementary Fig. 14).
1536
1537 d: Experiment as in a) was analysed by chromatin isolation and immunoblotting with the
1538 indicated antibodies. Coomassie staining of the gel part containing histones served as a loading
1539 control.
1540
1541
1542 **Figure 7: Exclusive binding of TopBP1 and DNA polymerase epsilon to GINS in the CMG**
1543 **context.**
1544
1545 a/b: Structure of human CMG (PDB 7PFO), in panel a with our GINS-TopBP1 superposed, in
1546 panel b with DNA Polε (CMGE; PDB 7PFO) both shown from the same angle, demonstrating

accessibility of the TopBP1 binding sites in CMG, and strong overlap between BRCT4 and PolE2 occupied spaces. The pink volume constitutes surface representation.

c: In-detail views of GINS-TopBP1 interaction sites from the cryo-EM model in this manuscript (8OK2) alongside the GINS-PolE2 interaction sites seen in the larger CMGE structure (7PFO).

Figure 1

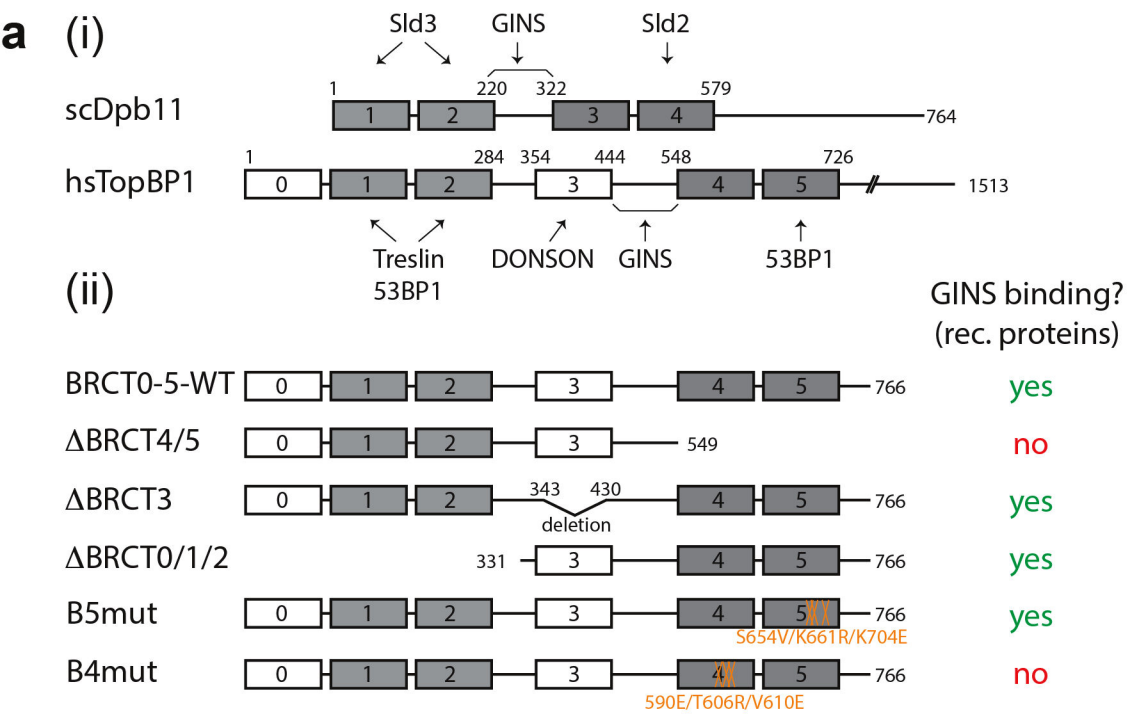
a
(i)
Sld3
GINS
Sld2
scDpb11
1
220
322
579
764
hsTopBP1
1
284
354
444
548
726
1513
Treslin
53BP1
DONSON
GINS
53BP1
(ii)
GINS binding?
(rec. proteins)
BRCT0-5-WT
766
yes
ΔBRCT4/5
549
no
ΔBRCT3
343
430
deletion
766
yes
ΔBRCT0/1/2
331
766
yes
B5mut
766
S654V/K661R/K704E
yes
B4mut
766
590E/T606R/V610E
no

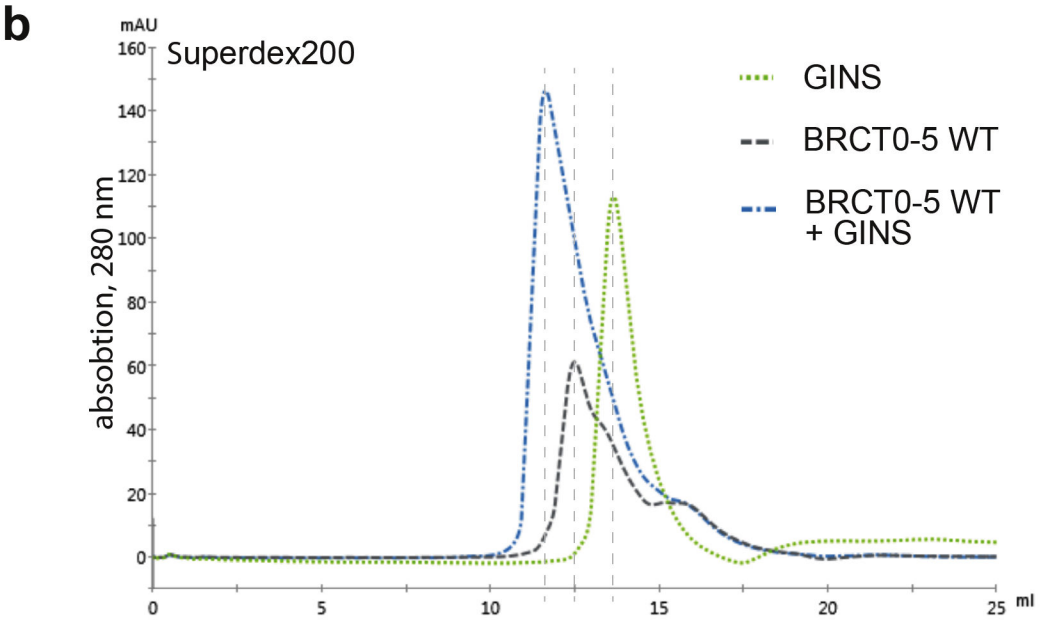
b
mAU
Superdex200
absobtion, 280 nm
GINS
BRCT0-5 WT
BRCT0-5 WT
+ GINS
ml

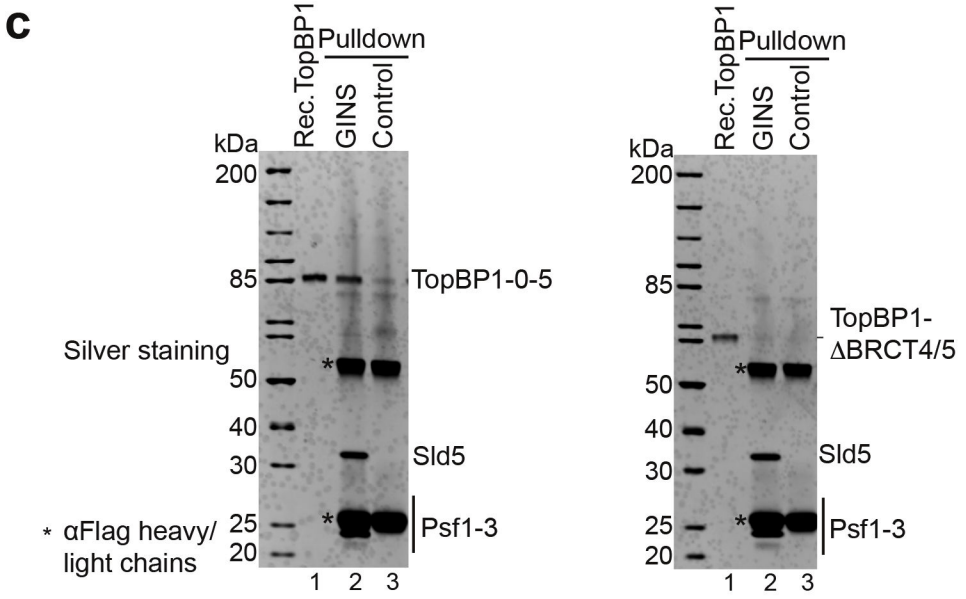
c
Rec. TopBP1
Pulldown
GINS
Control
kDa
200
85
50
40
30
25
20
Silver staining
TopBP1-0-5
Sld5
Psf1-3
* αFlag heavy/
light chains
1
2
3
TopBP1-
ΔBRCT4/5

Figure 2

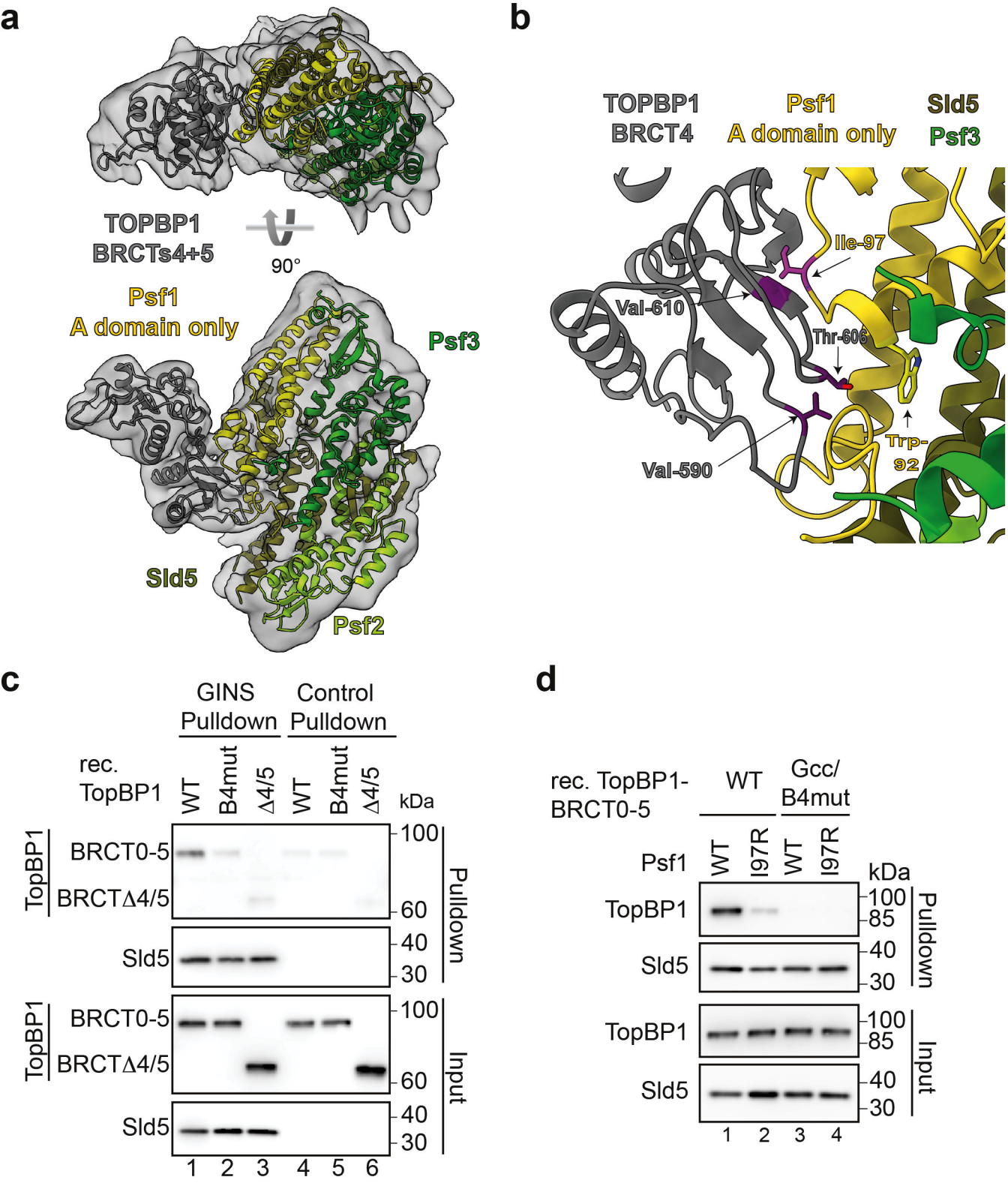
a
TOPBP1
BRCTs4+5
90°
Psf1
A domain only
Psf3
Sld5
Psf2
b
TOPBP1
BRCT4
Psf1
A domain only
Sld5
Psf3
Ile-97
Val-610
Thr-606
Trp-92
Val-590
c
GINS Pulldown
Control Pulldown
rec. TopBP1
WT
B4mut
Δ4/5
WT
B4mut
Δ4/5
kDa
TopBP1
BRCT0-5
BRCTΔ4/5
Sld5
100
60
40
30
Pulldown
Input
1 2 3 4 5 6
d
rec. TopBP1-BRCT0-5
WT
Gcc/B4mut
Psf1
WT
I97R
WT
I97R
kDa
TopBP1
Sld5
100
85
40
30
Pulldown
Input
1 2 3 4

Figure 3

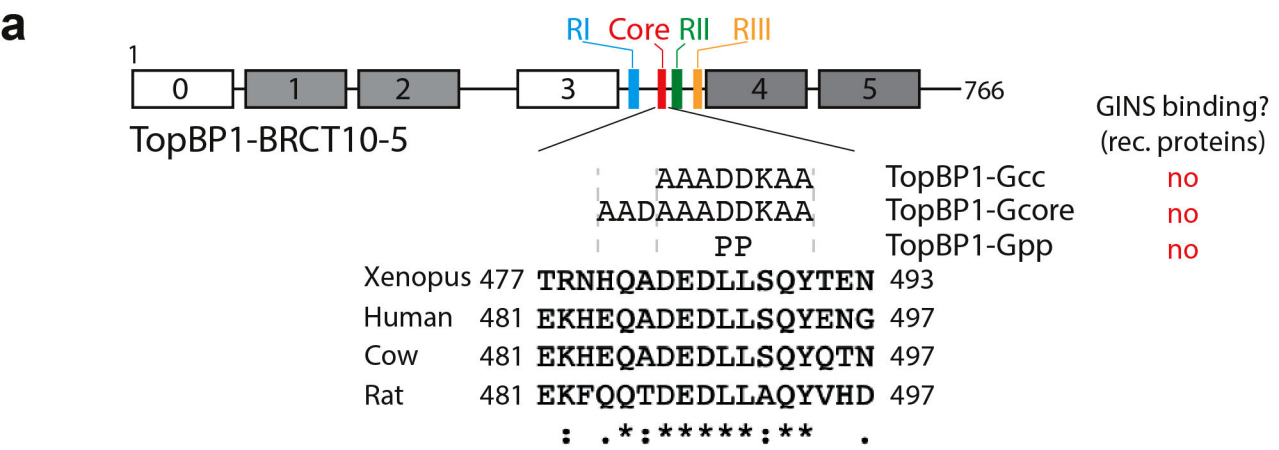
a
RI Core RII RIII
1
0 1 2 3 4 5
766
TopBP1-BRCT10-5
GINS binding?
(rec. proteins)
AAADDKAA TopBP1-Gcc no
AADAAADDKAA TopBP1-Gcore no
PP TopBP1-Gpp no
Xenopus 477 TRNHQADEDLLSQYTEN 493
Human 481 EKHEQADEDLLSQYENG 497
Cow 481 EKHEQADEDLLSQYQTN 497
Rat 481 EKFQQTDEDLLAQYVHD 497
: .*:*****:** .

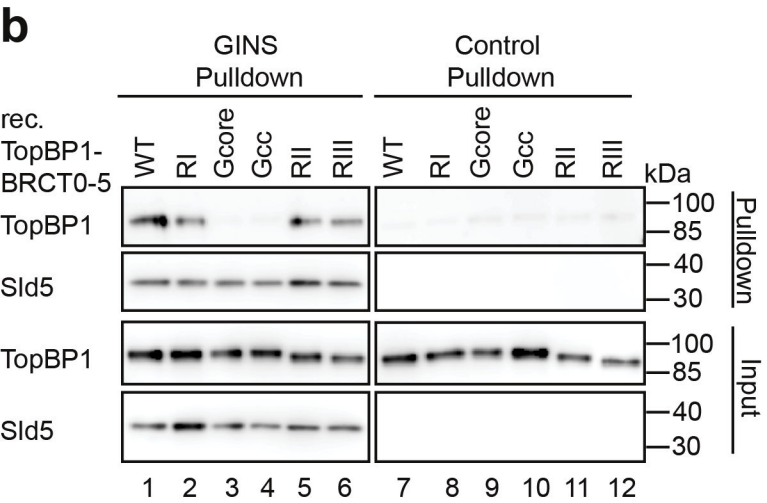
b
GINS Pulldown
Control Pulldown
rec. TopBP1-BRCT0-5
WT RI Gcore Gcc RII RIII WT RI Gcore Gcc RII RIII
kDa
TopBP1
Sld5
TopBP1
Sld5
100
85
40
30
Pulldown
Input
1 2 3 4 5 6 7 8 9 10 11 12

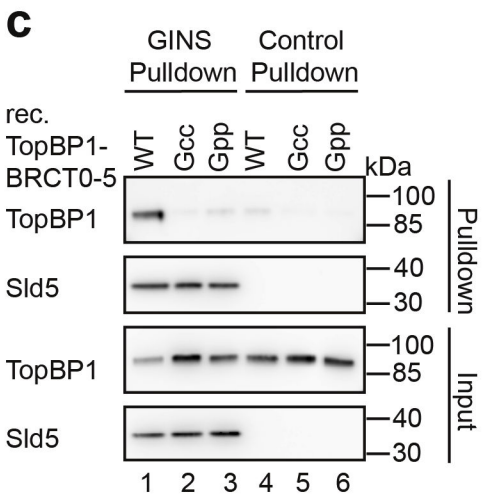
c
GINS Pulldown
Control Pulldown
rec. TopBP1-BRCT0-5
WT Gcc Gpp WT Gcc Gpp
kDa
TopBP1
Sld5
TopBP1
Sld5
100
85
40
30
Pulldown
Input
1 2 3 4 5 6

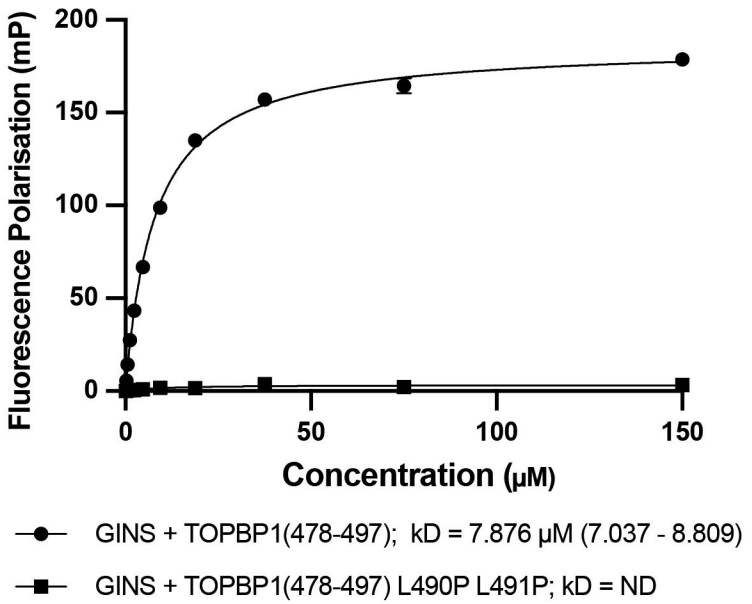
d
Fluorescence Polarisation (mP)
200
150
100
50
0
0
50
100
150
Concentration (μM)
GINS + TOPBP1(478-497); kD = 7.876 μM (7.037 - 8.809)
GINS + TOPBP1(478-497) L490P L491P; kD = ND

Figure 4

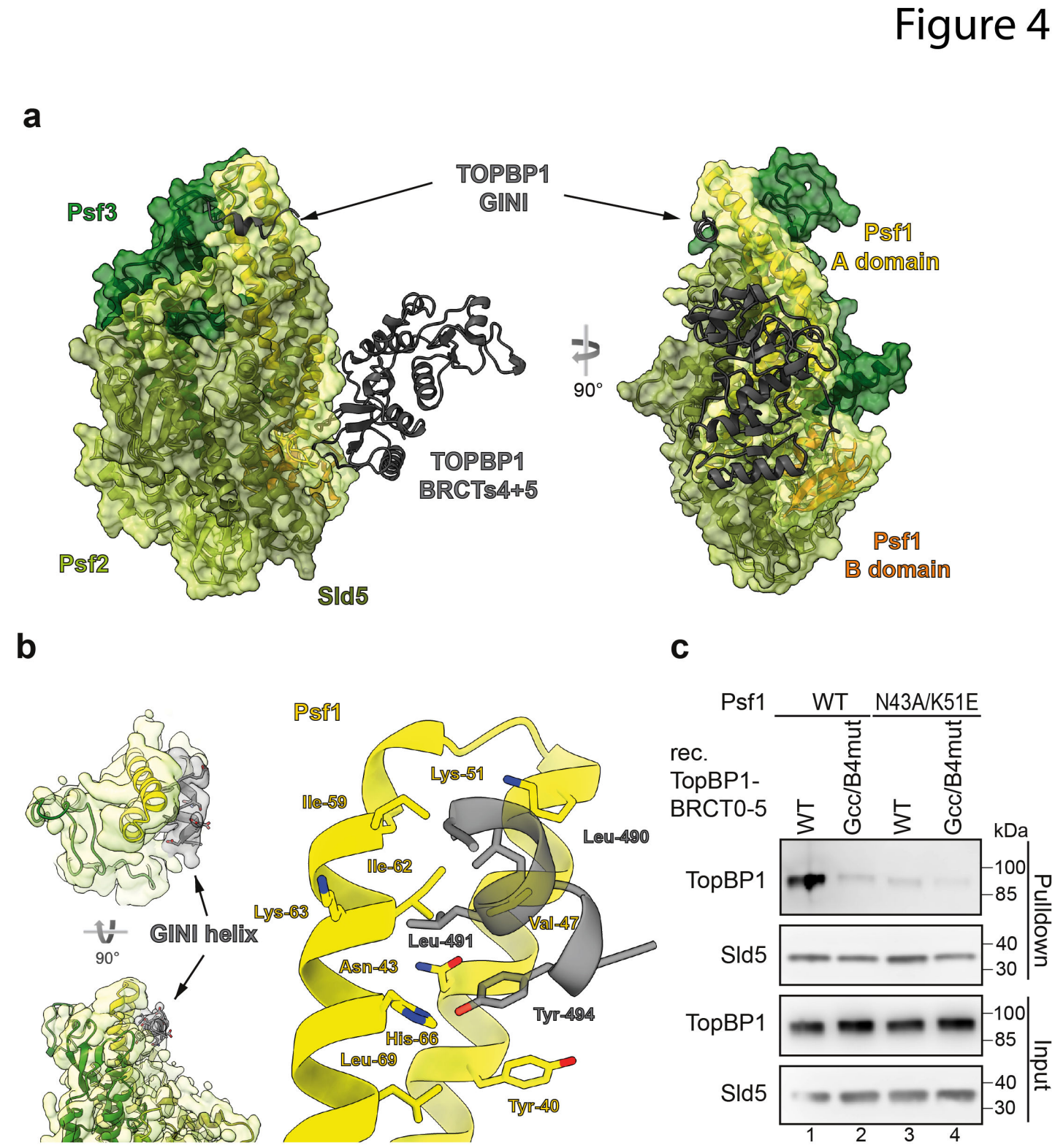
a
TOPBP1
GINI
Psf3
Psf1
A domain
90°
TOPBP1
BRCTs4+5
Psf2
Sld5
Psf1
B domain
b
Psf1
Lys-51
Ile-59
Leu-490
Ile-62
Lys-63
Val-47
GINI helix
90°
Leu-491
Asn-43
Tyr-494
His-66
Leu-69
Tyr-40
c
Psf1
WT
N43A/K51E
rec.
TopBP1-
BRCT0-5
WT
Gcc/B4mut
WT
Gcc/B4mut
kDa
TopBP1
100
85
Pulldown
Sld5
40
30
TopBP1
100
85
Input
Sld5
40
30
1
2
3
4

Figure 5

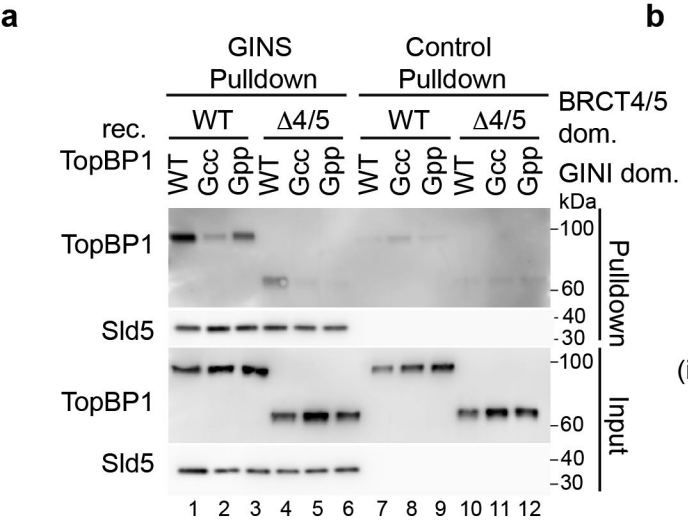

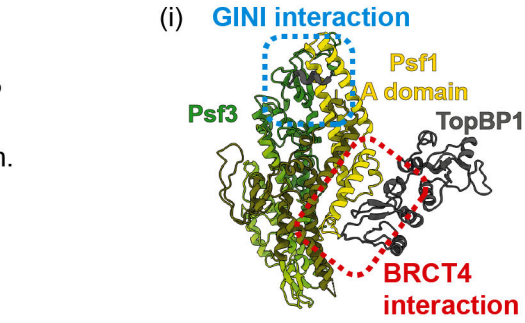

(ii)

interaction sites	Binding free energy [kcal/mol]	
	PPI-Affinity	PRODIGY
BRCT4 + GINI	-10.3	-15.0
BRCT4	-1.7	-8.4
GINI	-9.8	-10.9

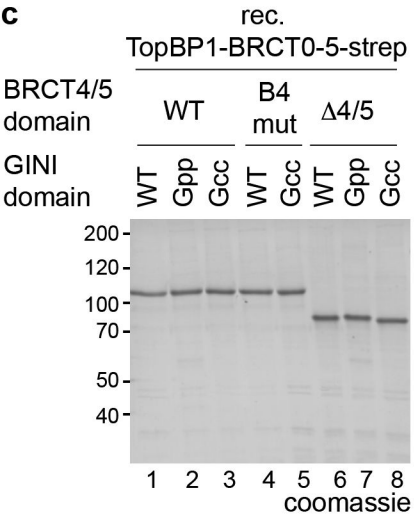

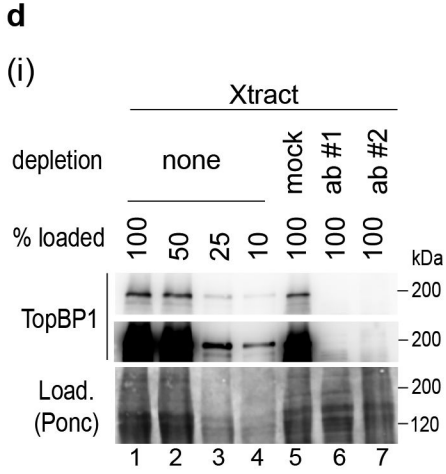

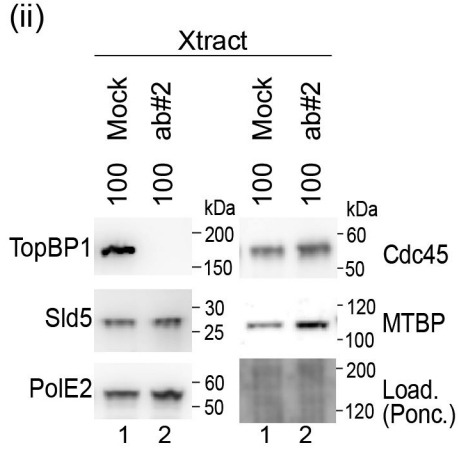

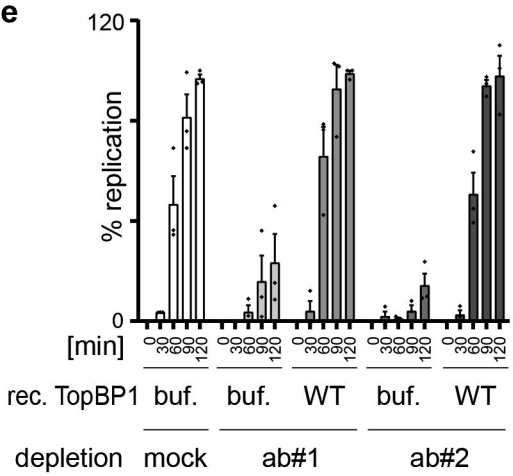

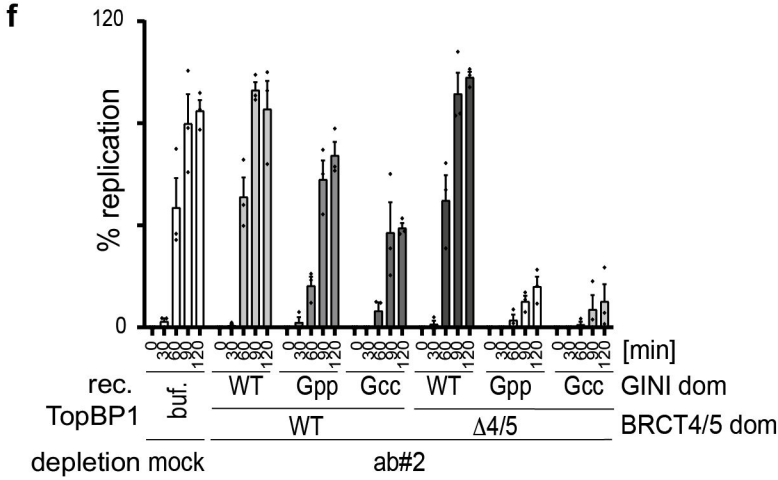

Figure 6

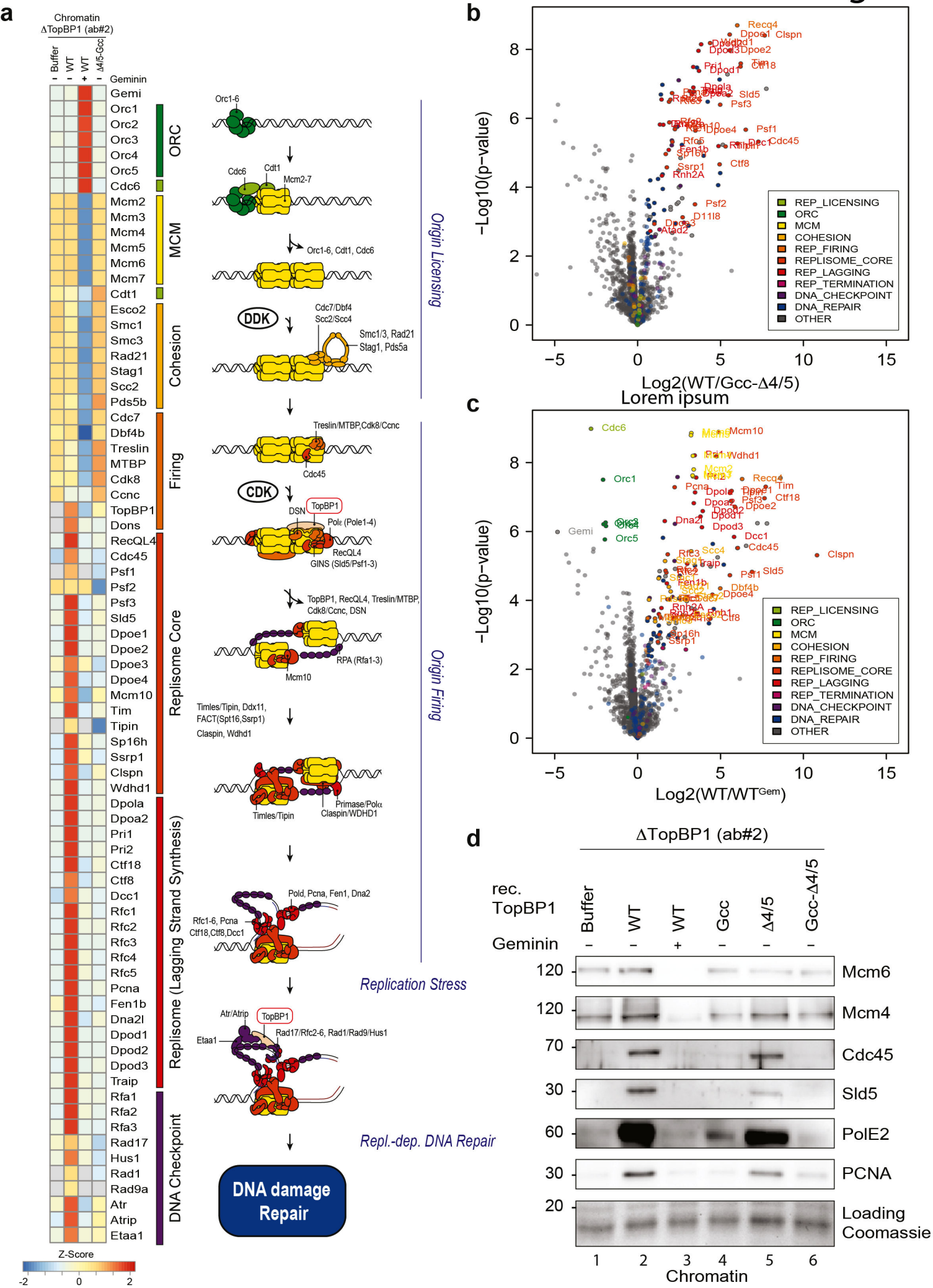
a
Chromatin
ΔTopBP1 (ab#2)
Buffer
WT
+ WT
Δ4/5-Gcc
Geminin
ORC
MCM
Cohesion
Firing
Replisome Core
Replisome (Lagging Strand Synthesis)
DNA Checkpoint
Z-Score
Origin Licensing
Origin Firing
Replication Stress
Repl.-dep. DNA Repair
DNA damage Repair
Orc1-6
Cdc6
Cdt1
Mcm2-7
Orc1-6, Cdt1, Cdc6
DDK
Cdc7/Dbf4
Scc2/Scc4
Smc1/3, Rad21
Stag1, Pds5a
Treslin/MTBP,Cdk8/Ccnc
Cdc45
CDK
DSN
TopBP1
Pole (Pole1-4)
RecQL4
GINS (Sld5/Psf1-3)
TopBP1, RecQL4, Treslin/MTBP, Cdk8/Ccnc, DSN
RPA (Rfa1-3)
Mcm10
Timles/Tipin, Ddx11, FACT(Spt16,Ssrp1)
Claspin, Wdhd1
Timles/Tipin
Primase/Polα
Claspin/WDHD1
Pold, Pcna, Fen1, Dna2
Rfc1-6, Pcna
Ctf18,Ctf8,Dcc1
Atr/Atrip
TopBP1
Rad17/Rfc2-6, Rad1/Rad9/Hus1
Etaa1
b
−Log10(p−value)
Log2(WT/Gcc-Δ4/5)
REP_LICENSING
ORC
MCM
COHESION
REP_FIRING
REPLISOME_CORE
REP_LAGGING
REP_TERMINATION
DNA_CHECKPOINT
DNA_REPAIR
OTHER
Lorem ipsum
c
−Log10(p−value)
Log2(WT/WTGem)
d
ΔTopBP1 (ab#2)
rec. TopBP1
Buffer
WT
+ WT
Gcc
Δ4/5
Gcc-Δ4/5
Geminin
Mcm6
Mcm4
Cdc45
Sld5
PolE2
PCNA
Loading Coomassie
Chromatin

Figure 7

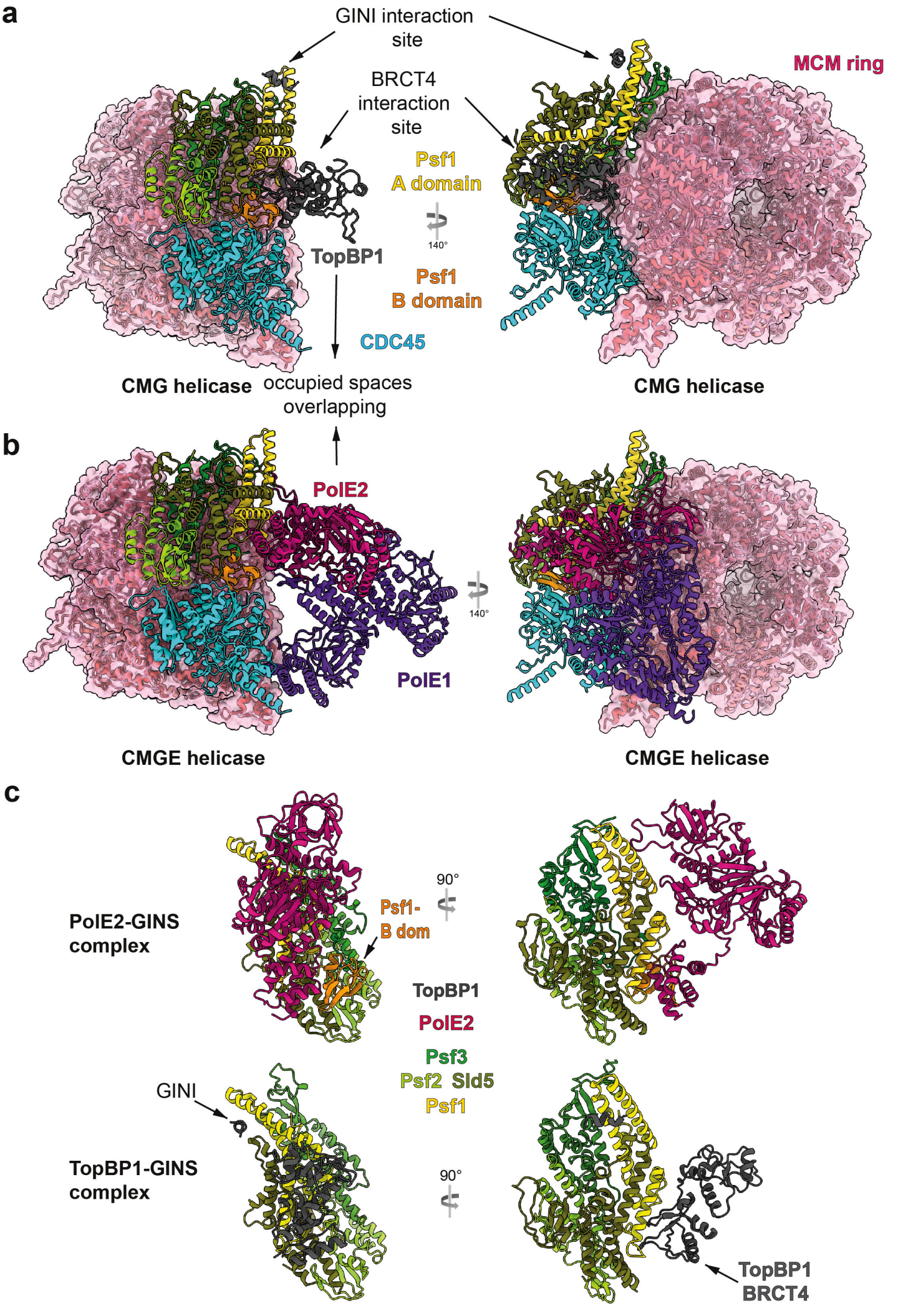
a
GINI interaction site
BRCT4 interaction site
MCM ring
Psf1 A domain
140°
TopBP1
Psf1 B domain
CDC45
CMG helicase
occupied spaces overlapping
CMG helicase
b
PolE2
140°
PolE1
CMGE helicase
CMGE helicase
c
PolE2-GINS complex
Psf1-B dom
90°
TopBP1
PolE2
Psf3
Psf2 Sld5
Psf1
GINI
TopBP1-GINS complex
90°
TopBP1 BRCT4